

Review

# High-Performance High-Nickel Multi-Element Cathode Materials for Lithium-Ion Batteries

Xinyong Tian<sup>1,2</sup>, Ruiqi Guo<sup>1,3</sup>, Ying Bai<sup>1</sup> , Ning Li<sup>4,5</sup>, Xinran Wang<sup>1,3,\*</sup>, Jiantao Wang<sup>4,5,\*</sup> and Chuan Wu<sup>1,3,\*</sup> 

<sup>1</sup> Beijing Key Laboratory of Environmental Science and Engineering, School of Materials Science & Engineering, Beijing Institute of Technology, Beijing 100081, China

<sup>2</sup> New Energy Materials Research Institute, Shaanxi Hongma Sci & Tech Co., Ltd., Hancheng 715400, China

<sup>3</sup> Yangtze Delta Region Academy of Beijing Institute of Technology, Jiaxing 314019, China

<sup>4</sup> China Automotive Battery Research Institute Co., Ltd., Beijing 100088, China

<sup>5</sup> General Research Institute for Nonferrous Metals, Beijing 100088, China

\* Correspondence: wangxinran@bit.edu.cn (X.W.); jiantaowang2002@126.com (J.W.);

chuanwu@bit.edu.cn (C.W.)

**Abstract:** With the rapid increase in demand for high-energy-density lithium-ion batteries in electric vehicles, smart homes, electric-powered tools, intelligent transportation, and other markets, high-nickel multi-element materials are considered to be one of the most promising cathode candidates for large-scale industrial applications due to their advantages of high capacity, low cost, and good cycle performance. In response to the competitive pressure of the low-cost lithium iron phosphate battery, high-nickel multi-element cathode materials need to continuously increase their nickel content and reduce their cobalt content or even be cobalt-free and also need to solve a series of problems, such as crystal structure stability, particle microcracks and breakage, cycle life, thermal stability, and safety. In this regard, the research progress of high-nickel multi-element cathode materials in recent years is reviewed and analyzed, and the progress of performance optimization is summarized from the aspects of precursor orientational growth, bulk phase doping, surface coating, interface modification, crystal morphology optimization, composite structure design, etc. Finally, according to the industrialization demand of high-energy-density lithium-ion batteries and the challenges faced by high-nickel multi-element cathode materials, the performance optimization direction of high-nickel multi-element cathode materials in the future is proposed.

**Keywords:** high energy density; lithium-ion battery; high-nickel multicomponent cathode material



**Citation:** Tian, X.; Guo, R.; Bai, Y.; Li, N.; Wang, X.; Wang, J.; Wu, C.

High-Performance High-Nickel Multi-Element Cathode Materials for Lithium-Ion Batteries. *Batteries* **2023**, *9*, 319. <https://doi.org/10.3390/batteries9060319>

Academic Editors: Wilhelm Pflöging and Ivana Hasa

Received: 25 March 2023

Revised: 23 May 2023

Accepted: 6 June 2023

Published: 9 June 2023



**Copyright:** © 2023 by the authors. Licensee MDPI, Basel, Switzerland. This article is an open access article distributed under the terms and conditions of the Creative Commons Attribution (CC BY) license (<https://creativecommons.org/licenses/by/4.0/>).

## 1. Introduction

Facing issues such as global warming and renewable resource shortages, countries around the world are paying more attention to the development of green environmental protection. In 2020, major economies around the world spoke out in support of the development of green environmental protection. The Chinese government also made a solemn commitment to the world at the 75th United Nations General Assembly, promising that China will achieve its carbon emission peak by 2030 and carbon neutrality by 2060. Carbon neutrality has become a consensus among all countries. Achieving energy cleanliness and electrification of transport are important ways to achieve carbon neutrality. The invention and application of lithium-ion batteries (LIBs) have made it possible for humans to achieve a society without fossil fuels. As a green and environmentally friendly energy storage device, LIBs have the advantages of high energy density, excellent cycle life, long endurance time, low self-discharge, no memory effect, and renewable recycling. They have been widely used in various portable electronic devices, household and outdoor wireless appliances, wireless power tools, new energy vehicles, electric logistics vehicles, household and outdoor energy storage, and other applications. Whether in mobile and portable products, new energy vehicles, or energy storage batteries, energy density has always been an important

indicator for LIBs. Therefore, it is necessary to develop and industrialize energy-dense electrode materials to meet the market demand for high performance LIBs [1–6].

High-nickel multi-element cathode materials belong to layered transition metal oxides, which are derived from lithium nickel oxide ( $\text{LiNiO}_2$ ). Currently, the most studied types are lithium nickel cobalt manganese oxide ( $\text{LiNi}_x\text{Co}_y\text{Mn}_{1-x-y}\text{O}_2$ , abbreviated as NCM) and lithium nickel cobalt aluminum oxide ( $\text{LiNi}_x\text{Co}_y\text{Al}_{1-x-y}\text{O}_2$ , abbreviated as NCA). Table 1 summarized the composition and properties of commonly used nickel-containing multi-element cathode materials. There are also some studies on lithium nickel cobalt oxide ( $\text{LiNi}_x\text{Co}_{1-x}\text{O}_2$ , abbreviated as NC), lithium manganese oxide ( $\text{LiNi}_x\text{Mn}_{1-x}\text{O}_2$ , abbreviated as NM), lithium nickel cobalt manganese aluminum oxide ( $\text{LiNi}_x\text{Co}_y\text{Mn}_z\text{Al}_{1-x-y-z}\text{O}_2$ , abbreviated as NCMA), lithium manganese aluminum oxide ( $\text{LiNi}_x\text{Mn}_y\text{Al}_{1-x-y}\text{O}_2$ , abbreviated as NMA), lithium aluminum oxide ( $\text{LiNi}_x\text{Al}_{1-x}\text{O}_2$ , abbreviated as NA), etc. In general, the high-nickel multi-element cathode materials generally refer to cathodes with a Ni molar fraction  $\geq 0.6$ . In applications such as the new energy vehicle market, high-nickel multi-element cathode materials are gradually improving their price/performance ratio by increasing their nickel content while reducing their cobalt content or becoming cobalt-free. However, they still face challenges, such as poor structural stability, surface microcracks and particle fragmentation, rapid decay in cycle life, poor thermal stability, and poor safety performance (Figure 1) [7–15]. Herein, this paper firstly introduces the structural characteristics of high-nickel multi-element cathodes, followed by a comprehensive analysis of their research progress in recent years, including precursor growth orientation regulation, bulk phase doping, surface coating modification, and crystal structure optimization. In addition, we also discuss the challenges and future research directions of high-nickel multi-element cathode materials to meet the urgent demand for LIBs with high capacity, long lifespan, high safety, and low cost.

**Table 1.** The composition and properties of commonly used nickel-containing multi-element cathode materials.

Materials	Abbreviation	Molar Fraction of Ni Element	Molar Fraction of Co Element	Molar Fraction of Mn Element	Molar Fraction of Al Element	Initial Discharge Capacity ( $\text{mAh g}^{-1}$ )
$\text{LiNi}_{1/3}\text{Co}_{1/3}\text{Mn}_{1/3}\text{O}_2$	NCM111	1/3	1/3	1/3	/	~153
$\text{LiNi}_{0.5}\text{Co}_{0.2}\text{Mn}_{0.3}\text{O}_2$	NCM523	0.5	0.2	0.3	/	~162
$\text{LiNi}_{0.6}\text{Co}_{0.2}\text{Mn}_{0.2}\text{O}_2$	NCM622	0.6	0.2	0.2	/	~169
$\text{LiNi}_{0.7}\text{Co}_{0.2}\text{Mn}_{0.1}\text{O}_2$	NCM721	0.7	0.2	0.1	/	~189
$\text{LiNi}_{0.8}\text{Co}_{0.1}\text{Mn}_{0.1}\text{O}_2$	NCM811	0.8	0.1	0.1	/	~198
$\text{LiNi}_{0.9}\text{Co}_{0.05}\text{Mn}_{0.05}\text{O}_2$	NCM90	0.9	0.05	0.05	/	~231
$\text{LiNi}_{0.8}\text{Co}_{0.15}\text{Al}_{0.05}\text{O}_2$	NCA	0.8	0.15	/	0.05	~202

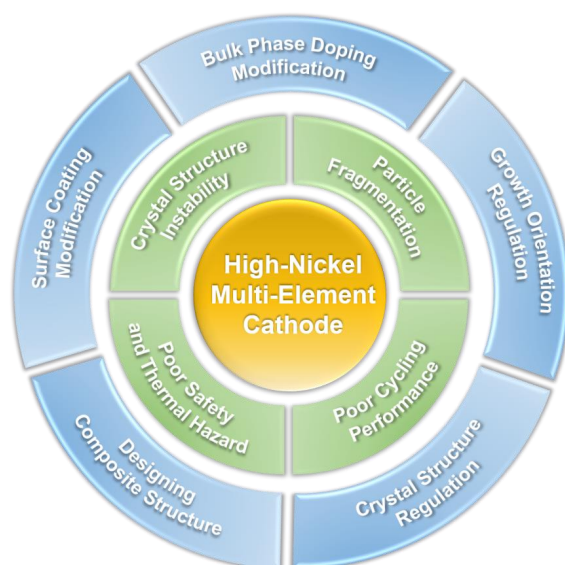


**Figure 1.** Challenges and research strategies faced by high-nickel multi-element cathode materials.

## 2. History and Structural Characteristics of High-Nickel Multi-Element Cathode Materials

Prior to the emergence of a multi-element cathode materials system, there were already cathode materials such as  $\text{LiCoO}_2$ ,  $\text{LiNiO}_2$ , and  $\text{LiMnO}_2$  that only contained Ni, Co, and Mn as a single component. With the further development of LIBs, cathode materials containing only Ni, Co, and Mn single elements gradually exposed their respective drawbacks and thus were unable to meet the requirements for high-performance LIBs. Researchers attempted to combine multiple elements into the same cathode material, resulting in the emergence of ternary cathode materials (NCM and NCA). The earliest ternary cathode material was designed by Liu et al. in 1999 [7]. They found that the NCM ternary cathode material has a more regular layered structure, which can greatly improve its cycle life compared to  $\text{LiNiO}_2$ . In 2001, Ohzuku et al. [8] prepared  $\text{Li}(\text{Ni}_{1/3}\text{Co}_{1/3}\text{Mn}_{1/3})\text{O}_2$  cathode with a Ni:Co:Mn ratio of 1:1:1 by spray pyrolysis. The reversible capacity of this material can reach  $184 \text{ mAh g}^{-1}$ , and the capacity retention rate can maintain 78% after 100 cycles at 3 C rate. The emergence of ternary cathode materials synergized the advantages of Ni, Co, and Mn, significantly improving the specific capacity, cycling, and rate performance of electrodes. Since then, the ternary material system has gradually entered the perspective of researchers. The development trend of ternary cathode materials is gradually shifting from low nickel NCM333, NCM424, NCM523, NCM622, etc., to high-nickel NCM712, NCM811, NCA, etc.

The crystal structures of NCM and NCA are consistent with that of  $\text{LiNiO}_2$ , with a hexagonal crystal system, an  $R3m$  space group, and an  $\alpha\text{-NaFeO}_2$  rock salt structure. The structural stability, reversible capacity, cycle life, safety, and other properties of high-nickel multi-element cathode materials are related to the synergy between multiple metal elements. In 1999, Liu et al. [7] investigated the synthesis of NCM523, NCM622, and NCM721 ternary cathode materials by co-doping Mn and Ni to replace some of the Ni, where Li atoms occupy the 3a position, Ni, Co, and Mn atoms occupy the 3b position, and O atoms occupy the 6c position. Ni, Co, Mn, and the six surrounding O atoms form a  $\text{MO}_6$  octahedral structure, with Li embedded between the oxide layer formed by the transition metal Ni, Co, Mn, and O atoms. The NCM ternary cathode materials have a more complete layered structure, and their cycle life can be greatly improved compared with  $\text{LiNiO}_2$ .

It was found that in the high-nickel multi-element cathode material NCA, the valence state of Ni is higher than that in NCM in order to maintain the total valence balance due to the substitution of the Al element for Mn [16–19]. In addition, Al has the characteristics of stable valence state during charging and discharging and small ionic radius easily and uniformly doped in the transition metal layer, and the Al–O bonding energy is greater than that of Mn–O. Therefore, the clustering phenomenon similar to that of  $\text{Mn}^{4+}$  in NCM materials does not occur in NCA. The introduction of Al can increase the ordered arrangement of the cathode crystal structure of NCA, reduce the Jahn–Teller effect distortion, lattice expansion, and contraction during charging and discharging, and improve the layered crystal structure and thermal stability.

## 3. Current Issues of High-Nickel Multi-Element Cathode Materials

### 3.1. Poor Stability of the Crystal Structure

The reversible specific capacity of high-nickel multi-element cathode increases as the nickel content increases. However, the high-nickel content can also lead to lithium–nickel disorder during high-temperature sintering due to the close radius of  $\text{Ni}^{2+}$  and  $\text{Li}^+$  ions [14–20], resulting in a decrease in the stability of the crystal structure and structural phase transition, which thereafter affects the diffusion rate of  $\text{Li}^+$  ions during cycling. Generally, the crystal structure phase transition occurs initially on the surface of the cathode material, transitioning from a layered structure to a spinel structure and finally turning into a nonactive rock salt phase. In order to maintain the valence equilibrium, the oxygen will precipitate out [21–43], leading to the deterioration of the thermal stability and a safety hazard. In severe cases, microcracks or fractures will appear inside the particles, leading to more side reactions between the

electrolyte and the cathode material and further affecting the insertion and extraction rate of  $\text{Li}^+$  ions [44–51].

Sun et al. [52] investigated the high-nickel multi-element cathode  $\text{LiNi}_{0.95}\text{Co}_{0.025}\text{Mn}_{0.025}\text{O}_2$  with ultrahigh capacity and compared it comprehensively with an  $\text{LiNiO}_2$  cathode. The specific capacity at 4.3 V is  $238 \text{ mAh}\cdot\text{g}^{-1}$ , and the capacity retention rate after 100 cycles is 85%, significantly higher than the 74% retention rate of  $\text{LiNiO}_2$  (Figure 2). The analysis of  $dQ/dV$  curves for different cycles showed that there were multiple phase transitions in the high-nickel cathode material, and the intensity of the oxidation–reduction peak of  $\text{LiNi}_{0.95}\text{Co}_{0.025}\text{Mn}_{0.025}\text{O}_2$  was much weaker, indicating that the introduction of Co and Mn can effectively improve the structural stability of high-nickel cathodes. The cycling retention and DSC thermal stability data can also support the above conclusions. Moreover, their study found that the main reason for the rapid decay of the capacity of  $\text{LiNi}_{0.95}\text{Co}_{0.025}\text{Mn}_{0.025}\text{O}_2$  was the anisotropy of lithium ions during the charge and discharge cycle and the volume change of the crystal grains, which led to a deterioration in the crystal structure. The uneven micro-stresses within the particles caused the formation of microcracks (see Figure 2e–h), accelerating the penetration of the electrolyte into the secondary particles, leading to severe irreversible phase transitions, particle disintegration, and a rapid decline in battery performance.

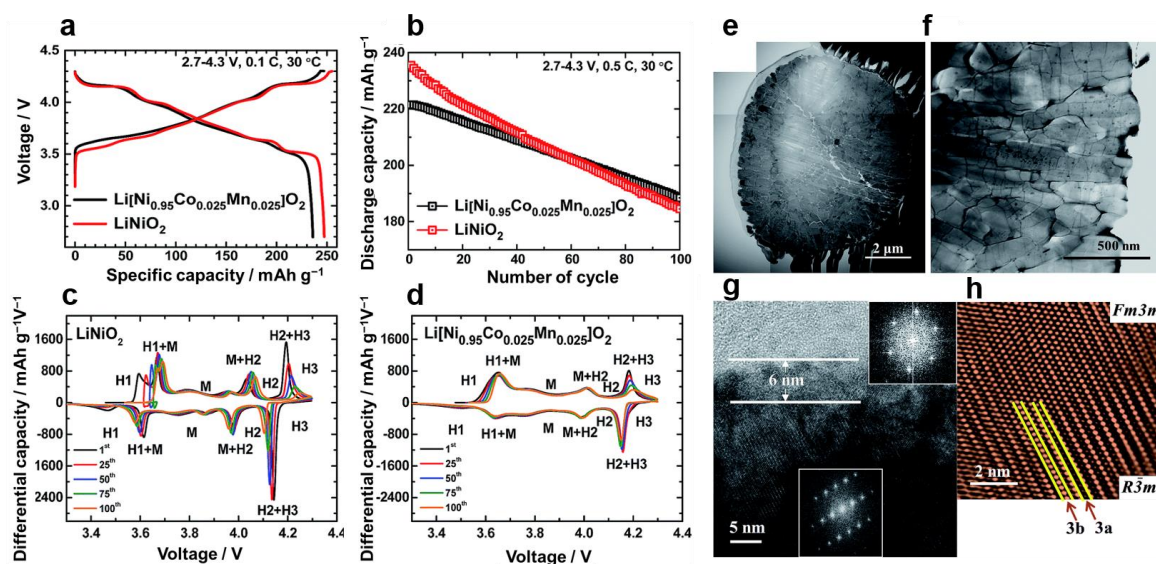


**Figure 2.** (a) Initial charge and discharge curves at 2.7–4.3 V, 0.1 C, 30 °C with a 2032 coin cell using a Li metal anode, (b) cycling curves at 0.5 C, (c)  $dQ/dV$  curves of  $\text{LiNiO}_2$ , (d)  $dQ/dV$  curves of  $\text{LiNi}_{0.95}\text{Co}_{0.025}\text{Mn}_{0.025}\text{O}_2$ , (e) bright-field scanning TEM of a cross-section from the  $\text{LiNi}_{0.95}\text{Co}_{0.025}\text{Mn}_{0.025}\text{O}_2$  after 100 cycles, (f) dark-field scanning TEM image of  $\text{LiNi}_{0.95}\text{Co}_{0.025}\text{Mn}_{0.025}\text{O}_2$ , (g) High-resolution TEM image with Fourier transforms of the interior and surface regions, (h) Fourier-filtered TEM of the transient region transforming. Reproduced with permission [52]. Copyright (2018) Royal Society of Chemistry.

Liang et al. [16] used first principles and DFT to establish a TM-TM ion interaction model between NiCoMn transition metals and studied the effect of structural stability on the high-nickel multi-element cathode material  $\text{LiNi}_{1-2x}\text{Co}_x\text{Mn}_x\text{O}_2$  ( $x < 0.2$ ). The bond strength of the TM-TM bonds was determined to be  $\text{Ni}^{2+}\text{-Mn}^{4+} > \text{Ni}^{3+}\text{-Mn}^{4+} > \text{Co}^{3+}\text{-Mn}^{4+} > \text{Co}^{3+}\text{-Co}^{3+} > \text{Ni}^{3+}\text{-Ni}^{3+} > \text{Mn}^{3+}\text{-Mn}^{3+}$ . From the order of bond strength, it can be inferred that the structural stability of high-nickel NCM811 with low-bond-energy  $\text{Ni}^{3+}\text{-Mn}^{4+}$  and  $\text{Ni}^{3+}\text{-Ni}^{3+}$  is lower than that of low-nickel NCM523 with high-bond-energy  $\text{Ni}^{2+}\text{-Mn}^{4+}$  and  $\text{Co}^{3+}\text{-Mn}^{4+}$ . The research results showed that when  $\text{Ni} \geq 0.80$ , Co and Mn ions tend to form cluster phenomena, resulting in transition metal segregation and poor crystal structure stability of the material. The  $\text{Co}^{3+}/\text{Co}^{4+}$  transition provides additional capacity when high-nickel multi-element cathodes de-lithium at high voltages of 4.3 V. In order to maintain

the valence balance, the oxygen atoms in the crystal structure will precipitate, leading to structural collapse of the material, which results in rapid decline in battery capacity, high temperature, cycling, and safety performance.

### 3.2. Microcracking and Particle Fragmentation

Studies related to the performance degradation of high-nickel cathode materials [53–66] have shown that crystal structure phase changes, microcracking, and particle fragmentation are the main causes of performance degradation. The unstable crystal structure of high-nickel cathodes can be attributed to their high specific capacity and high proportion of lithium-ion insertion and extraction, which makes them vulnerable to lithium–nickel intermixing and structural phase transitions during cycling, leading to non-uniform stress changes. Moreover, anisotropic stress volume changes, resulting from the H2-H3 phase alteration in the crystal structure, can lead to microcracks at the grain boundaries within the particles. As the number of cycles increases, microcracks on the surface of the particles increase and side reactions with the electrolyte occur, resulting in particle fragmentation and leaching of transition metals. Furthermore, it has also been observed that increasing the Ni content in high-nickel cathode materials can lead to greater crystal volume change ( $\Delta V$ ), cause the severe formation of microcracks and particle fragmentation, and accelerate capacity degradation.

Wu et al. [67] employed synchrotron X-ray computed tomography and the three-dimensional finite element method to investigate the stress generated by lithium-ion insertion and structural phase transition in the NCM. The study identified that microcracks were generated on the particle surface, and the accumulation of structural phase transition within the particles during prolonged cycling gradually increased the stress of the material particles, resulting in particle breakage and rapid degradation of battery performance. Additionally, Sun et al. [68] investigated the capacity degradation mechanism of NCM with different Ni contents (0.8, 0.88, 0.95). The study indicated that as the Ni content increased, the discharge specific capacity of the cathode material increased, but the number of microcracks within the particles gradually increased, resulting in a decrease in cycle retention rate and DSC decomposition temperature. The degree of cycle capacity degradation is linked to the degree of microcracks caused by the anisotropic volume change resulting from the H2-H3 phase transition. The result suggested that adjusting the nickel content in the cathode material can achieve excellent electrical performance and safety performance. Additionally, they also proposed to reduce the anisotropic volume change during the H2-H3 phase transition of the cathode by designing long rod-shaped and well-crystallized materials. Later, Sun et al. [69] systematically investigated the capacity degradation mechanism of two high-nickel cathode materials (NCM811 and NCM90). The study revealed that mechanical degradation caused by microcracks was the primary reason for the performance deterioration of high-nickel cathode material; microcracks in the internal area of the particles aggravated the erosion of the electrolyte and accelerated the rapid degradation of electrochemical performance and structure. Compared to the NCM811 cathode material, the particle surface microcracking phenomenon is further exacerbated in NCM90. The surface microcracks provide channels through which the electrolyte can penetrate, resulting in significantly faster cycling capacity degradation in NCM90.

### 3.3. Poor Thermal Stability and Safety

Yoon et al. [70] systematically investigated the thermal stability of high-nickel cathode materials. Due to the high proportion of de-lithiation at the same potential of high-nickel cathodes, it leads to an increase in  $\text{Ni}^{4+}$  content and can be easily reduced to  $\text{Ni}^{3+}$ . Since  $\text{Ni}^{3+}$  and  $\text{Co}^{3+}$  have overlapping electronic energy bands with O atoms, the O atoms will precipitate out of the lattice in the high de-lithiation state to release a certain amount of oxygen and destroy the crystal structure. The transformation of its particle surface from the layer into the spinel phase and further rock salt phase occurs, leading to rapid decay in the thermal stability and cycling capacity of the battery, which can easily lead to explosions, fire,

and other safety hazards. Therefore, the structural phase change and oxygen precipitation of high-nickel cathode materials is one of the main reasons for the poor thermal stability of the LIBs [71–81].

Noh et al. [77] investigated the effect of different nickel contents of ternary cathode materials  $\text{LiNi}_x\text{Co}_{1-2x}\text{MnO}_2$  ( $x = 1/3, 0.5, 0.6, 0.7, 0.8, 0.85$ ) on crystal structure, thermal stability, and electrochemical properties. The residual base, ionic conductivity, and specific capacity of the cathode material increase with higher nickel content (Figure 3). However, the cycling performance, thermal stability, and DSC thermal decomposition temperature of the cathode material become lower with the increase in nickel content. Sun et al. [78] also studied the thermal stability of multi-element cathode materials with different nickel contents. They found that as the nickel content increased, the thermal stability of the material became progressively worse, and the DSC oxygen precipitation decomposition temperature of the material gradually decreased. These findings suggest that the optimization of nickel content is crucial for achieving a balance between high capacity and good thermal stability in cathode materials. Sun et al. [79] investigated the causes of battery performance degradation of NCM811 under overcharging conditions using a variety of methods, including  $^{18}\text{O}$  isotope labelling, OEMS characterization methods, in situ and ex situ spectroscopy, and electron microscopy techniques. The data showed that the degradation of NCM811 under overcharging conditions mainly originates from the collapse of the cathode material, the precipitation of oxygen, which mainly occurs on the surface of the primary particles, and the formation of voids in the grain boundary region. As the crystal structure changes, microcracks appear inside and on the surface of the particles, accelerating the side reaction with the electrolyte and generating large amounts of oxygen, posing a serious safety hazard for the battery.

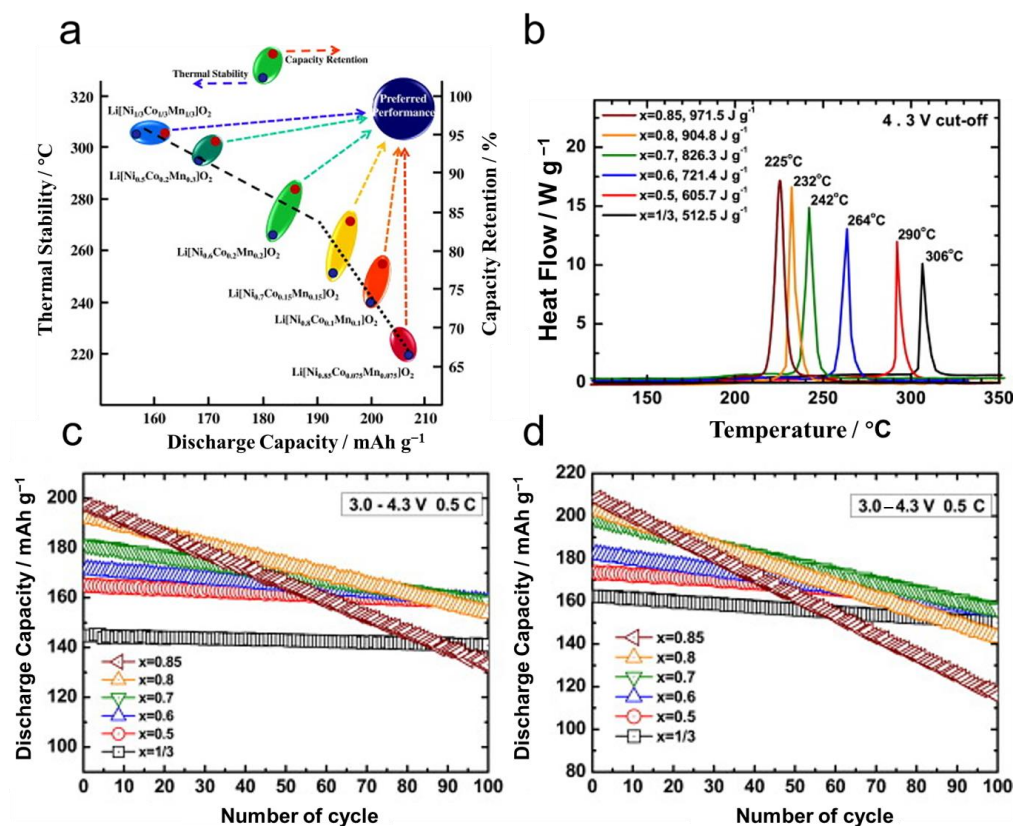


**Figure 3.** (a) A map of the relationship between discharge capacity, thermal stability, and capacity retention of  $\text{LiNi}_x\text{Co}_y\text{Mn}_z\text{O}_2$  ( $x = 1/3, 0.5, 0.6, 0.7, 0.8, 0.85$ ), (b) DSC curves, (c) 0.5 C cycle curves of the  $\text{LiNi}_x\text{Co}_y\text{Mn}_z\text{O}_2$  ( $x = 1/3, 0.5, 0.6, 0.7, 0.8, 0.85$ ) at 25  $^{\circ}\text{C}$ , (d) 0.5 C cycle curves of the  $\text{LiNi}_x\text{Co}_y\text{Mn}_z\text{O}_2$  ( $x = 1/3, 0.5, 0.6, 0.7, 0.8, 0.85$ ) at 45  $^{\circ}\text{C}$ . Reproduced with permission [77]. Copyright (2013) Elsevier.

### 3.4. Poor Cycling Life Performance

High-nickel cathode materials have poor structural stability and are susceptible to lithium–nickel intermixing, structural phase transformation, microcracking, particle fragmentation, and transition metal dissolution, resulting in the rapid degradation of cycle life performance [80–84]. Watanabe et al. [28,54] conducted a systematic investigation of the cycling performance of NCA in relation to the depth of discharge in charge–discharge processes (DOD) using various methods, such as XPS, XRD, and SEM. The cycling performance of the battery was excellent at 25 °C and remained acceptable even at 60 °C when the DOD was in the range of 10–70%. However, an increase in the DOD led to faster microcrack generation on the surface of the cathode and a faster battery cycling decay. Microcrack generation on the particle surface and the growth of NiO-like layers, which form the Fm3m rock salt structure, are the primary causes of capacity decay in NCA. Hayashi et al. [80] investigated and analyzed the cycle life decay mechanism of commercialized  $\text{LiNi}_{0.82}\text{Co}_{0.15}\text{Al}_{0.03}\text{O}_2$  by combining electrochemical tests with spherical differential-corrected scanning transmission electron microscopy (Cs-STEM), electron energy loss spectroscopy (EELS), and X-ray photoelectron spectroscopy (XPS). It was found that the surface of the cathode active material showed significant degradation after cycling tests. Most of the low valence Ni was present on the surface of the cathode material, which was charged after the cycling test, and the degraded surface layer was inactive to the charge reaction. Therefore, the degraded surface layer will accelerate the decay of the cycling performance of LIBs during long-term cycling tests.

Sun et al. [81] synthesized various high-nickel cathode materials, including  $\text{LiNi}_{0.85}\text{Co}_{0.00}\text{MnO}_{0.152}$ ,  $\text{LiNi}_{0.85}\text{Co}_{0.05}\text{Mn}_{0.10}\text{O}_2$ ,  $\text{LiNi}_{0.85}\text{Co}_{0.10}\text{Mn}_{0.05}\text{O}_2$ , and  $\text{LiNi}_{0.85}\text{Co}_{0.15}\text{Mn}_{0.00}\text{O}_2$ , with different Co/Mn ratios using co-precipitation. The effects of the Co/Mn ratios on the capacity, rate performance, cycling, and thermal stability were investigated. The results showed that as Co and Mn decreased, both the rate performance and thermal stability deteriorated. The cycling performance was better with a relatively higher Mn content. Among the different cathode materials,  $\text{LiNi}_{0.85}\text{Co}_{0.10}\text{Mn}_{0.05}\text{O}_2$  exhibited the most promising electrochemical performance, with a high capacity of approximately  $163 \text{ mAh}\cdot\text{g}^{-1}$  at 5 C and good thermal stability (with an exothermic temperature and exothermic heat of 233.7 °C and  $857.3 \text{ J g}^{-1}$ , respectively). Kim et al. [82] investigated the cycling decay mechanism of NCM811 and observed a 16.3% capacity loss during a 300-cycles test of a soft-pack full cell. The disassembled high-nickel cathode material after 1, 100, 200, and 300 cycles was analyzed. The discharge capacity of the half-cell after one week of cycling was  $208.4 \text{ mAh}\cdot\text{g}^{-1}$ , and the capacity retention rate after 300 cycles was 93.0%. FESEM analysis showed microcrack formation in the high-nickel secondary particles during cycling. The increase in interfacial area caused by microcracking led to side reactions between the material and the electrolyte, resulting in capacity degradation. The mechanical strength of the secondary particles significantly reduced after full-cell cycling due to the particle strength reduction of high-nickel cathode materials. Therefore, particle strength must be considered during the preparation of high-nickel cathode materials to prevent capacity decay during cycling.

## 4. Performance Optimization of High-Nickel Multi-Element Cathode Materials

In light of the issues regarding the poor crystal structure stability, microcracks and particle breakage, low thermal stability and safety performance, and rapid cycling life decay of high-nickel multi-element cathode materials, this article aims to summarize and analyze the recent progress made by scientific researchers in optimizing the performance of high-nickel cathodes. The next section summarizes and analyzes the recent research work on high-nickel cathodes in terms of precursor growth orientation control, bulk phase doping structure control, surface coating interface modification, crystal morphology optimization control, and material composite structure design.

#### 4.1. Regulation of Growth Orientation of Precursor

The primary raw materials for synthesizing high-nickel cathode materials are a precursor and lithium salt, with the former requiring customized synthesis according to the performance requirements of the high-nickel cathodes. Currently, the most common method for synthesizing precursors in research and industrial applications is co-precipitation [85–99]. This method controls the parameters of reaction pH, reaction temperature, solid content, salt concentration and flow rate, ammonia concentration and flow rate, alkali concentration and flow rate, impeller structure, stirring speed, reaction atmosphere, and reaction mode and utilizes aggregation, dissolution, and recrystallization to synthesize precursors with a specific morphology, particle size, particle size distribution, tap density, specific surface area, and impurity content, among other indicators.

Yang et al. [90] utilized the co-precipitation method to synthesize NCM622 precursors with different internal structural morphologies by controlling the pH and ammonia concentration. The sintered cathode material effectively inherited the structural morphology of the precursor, as demonstrated in Figure 4. The study found that regulating parameters, such as pH and ammonia concentration, during the precursor synthesis process can effectively control the growth orientation (HNC1) of the precursor's primary particles. This orientation results in the crystalline planes (010) and (100) of the sintered cathode material facing towards the surface of the cathode material particles. This orientation is mainly to reduce  $\text{Li}^+$  diffusion impedance, improve battery rate performance, and enhance the structural stability and cycling performance of the material during long cycling.

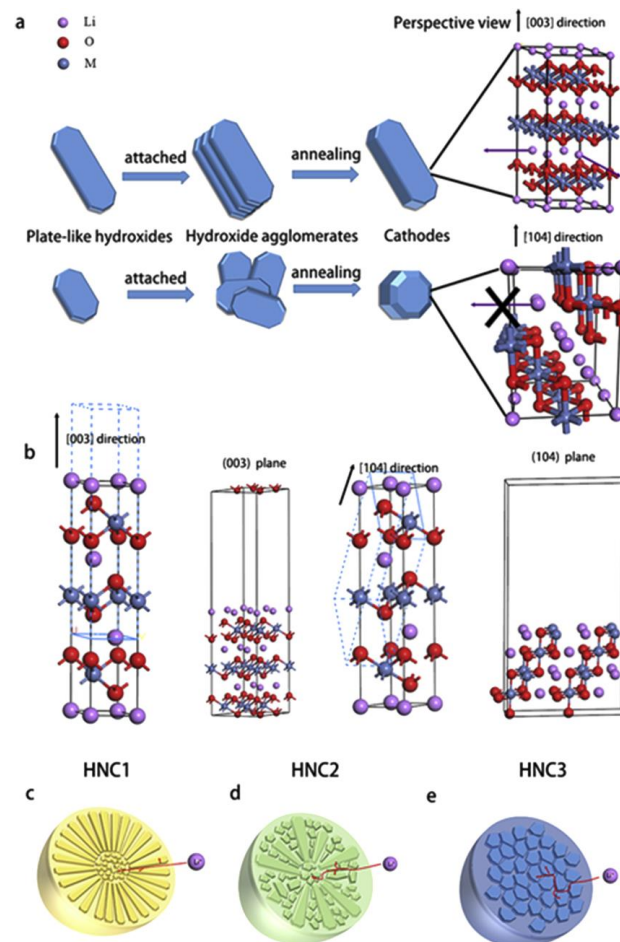


**Figure 4.** (a) Schematic illustration of ordered and disordered agglomerates and the microstructures of their surfaces. (b) Crystal model for calculating the surface energy of the (003) and (104) facet planes. Schematic illustration of three different internal structures: (c) HNC1, (d) HNC2, and (e) HNC3. Reproduced with permission [90]. Copyright (2016) Elsevier.

Hu et al. [91] synthesized high-surface-area  $\text{Ni}_{1-x-y}\text{Co}_x\text{Al}_y(\text{OH})_2$  hydroxides by co-precipitation and used excess LiOH calcination to prepare a high-nickel single crystal cathode multiphase material,  $\text{LiNi}_{0.8}\text{Co}_{0.15}\text{Al}_{0.05}\text{O}_2$ . The cathode showed an  $\alpha\text{-NaFeO}_2$  layered structure with a single-disperse micron-sized particle distribution and exhibited a high compacted density of  $3.8 \text{ g cm}^{-3}$ . The single-disperse micron-scale particles and high structural stability give the NCA an excellent compaction density and cycling capability. The excellent energy storage performance of the synthesized NCA microcrystals can be attributed to the reduced specific area, the rigid structure, and the homogeneous particle distribution.

Sun et al. [92] employed the co-precipitation method to synthesize  $\text{Ni}_{0.9}\text{Co}_{0.1}(\text{OH})_2$  precursor with two distinct morphologies to control the growth orientation of the precursor. They subsequently obtained  $\text{LiNi}_{0.86}\text{Co}_{0.1}\text{Al}_{0.04}\text{O}_2$ , with a high Al gradient concentration, while maintaining the inherited precursor morphology through sintering with an excess of Al doping and lithium salt mixture. This cathode maintained 86.5% of the initial capacity after 2000 cycles. The cathode also achieved an unprecedented 78.0% retention rate under the same conditions, even at a harsh operating condition of  $45^\circ\text{C}$ . The results suggest that microform and microstructural engineering modulation can effectively mitigate the capacity decay that affects the nickel-rich cathode during cycling.

Wu et al. [93] successfully synthesized NCM811 cathode materials with an exposed active (104) crystalline surface modulation by a co-precipitation process and a high-temperature lithiation reaction. In addition, the tightly adhered nanosheets on the (001) surface help to alleviate stress changes caused by the anisotropic structure and inhibit the fragmentation of secondary particles. The synthesized cathode material has excellent reversible discharge capacity ( $203.8 \text{ mAh}\cdot\text{g}^{-1}$  at 0.1 C) and stable cycling performance (89.3% capacity retention after 100 cycles at 1 C, 55.3% after 300 cycles at 5 C, and 59.6% after 300 cycles at 10 C).

#### 4.2. Structural Modification by Bulk Phase Doping

High-nickel cathode materials are prone to structural phase transitions during high voltage and long cycling processes, resulting in the rapid deterioration of battery performance. To address these issues, modification methods, such as bulk doping and surface coating, are commonly used. Bulk doping involves the introduction of trace dopant elements to replace some of the atoms in the crystal lattice, which can improve the M-O bond energy of the dopant element and further enhance the structural stability of the material. Bulk doping can reduce lithium–nickel intermixing, inhibit the transition of the NiO structure from a layered to a nonactive rock salt phase, and mitigate material microcracks and particle breakage, thus increasing the Li ion diffusion kinetics and enhancing the thermal stability and safety. Bulk doping can be generally divided into cation and anion doping. Metal elements, such as  $\text{Al}^{3+}$  [94–101],  $\text{Gd}^{3+}$  [102],  $\text{Zr}^{4+}$  [103–107],  $\text{Ti}^{4+}$  [108–110],  $\text{Ge}^{4+}$  [111],  $\text{Nb}^{5+}$  [112–116],  $\text{Ta}^{5+}$  [117–119],  $\text{Mo}^{6+}$  [120–123],  $\text{W}^{6+}$  [124–127],  $\text{Mg}^{2+}$  [128–136],  $\text{Ca}^{2+}$  [137],  $\text{Sr}^{2+}$  [138],  $\text{Zn}^{2+}$  [139], and  $\text{Na}^+$  [140–142], are commonly used, as well as non-metallic elements, such as B [143–146]. Anion doping is mostly conducted using halogens, such as  $\text{F}^-$  [147–151]. In addition, there are also composite doping methods, such as  $\text{LiAlF}_4$  [152],  $\text{NaF}$  [153],  $\text{Ga}+\text{B}$  [154],  $\text{Zr}+\text{B}$  [155,156],  $\text{Zr}+\text{Mg}$  [157], etc.

Among the various cation doping elements mentioned above,  $\text{Al}^{3+}$  is a commonly used doped metal element, while  $\text{Gd}^{3+}$  is relatively less used.  $\text{Al}^{3+}$  can increase the ordered arrangement of the crystal structure of the cathode material and reduce distortions such as the Jahn–Teller effect, lattice expansion and contraction during cycling, particle microcracks, and fragmentation. Manthiram et al. [96] synthesized high-nickel cathode materials  $\text{LiNi}_{0.7}\text{Co}_{0.15}\text{Mn}_{0.15}\text{O}_2$  (NCM71515), NCM811,  $\text{LiNi}_{0.9}\text{Co}_{0.05}\text{Mn}_{0.05}\text{O}_2$  (NCM90505),  $\text{LiNi}_{0.94}\text{Co}_{0.06}\text{O}_2$  (NC9406), and  $\text{LiNi}_{0.92}\text{Al}_{0.02}\text{Co}_{0.06}\text{O}_2$  (Al-NC9406). As the nickel content increases, the residual alkali content on the surface of the cathode material gradually increases. The residual alkali content of NC9406 with the highest nickel content is the highest. However, the use of Al-doped Al-NC9406 has the lowest residual alkali content and the

best stability, with significantly improved capacity retention and cycling performance. Sun et al. [97] synthesized three high-nickel cathode materials,  $\text{LiNi}_{0.90}\text{Co}_{0.05}\text{Mn}_{0.05}\text{O}_2$  (NCM90),  $\text{LiNi}_{0.888}\text{Co}_{0.097}\text{Al}_{0.015}\text{O}_2$  (NCA89), and  $\text{LiNi}_{0.89}\text{Co}_{0.05}\text{Mn}_{0.05}\text{Al}_{0.01}\text{O}_2$  (NCMA89), by co-precipitation and solid-phase high-temperature sintering. The NCMA89 was synthesized by doping Al elements into NCM(OH)<sub>2</sub> precursor compound and has a significantly improved structural stability and electrochemical performance compared to other cathodes. Comparative studies have shown that Al doping can effectively relieve surface microcracks and particle fragmentation problems of high-nickel cathode materials. The NCMA89 exhibited excellent cycling performance, with 85% capacity retention for 1000 weeks. Jiang et al. [98] designed the high-nickel cathode material  $\text{LiNi}_{0.9}\text{Co}_{0.1}\text{O}_2$  through gradient Al doping and surface  $\text{LiAlO}_2$  coating. The theoretical calculation, HT-XRD, and in situ XRD test results showed that  $\text{Al}^{3+}$  can reduce the transfer of  $\text{Ni}^{2+}$  to the Li layer, thereby inhibiting the transformation of H2–H3 phases, reducing volume deformation and internal stress. The coating of  $\text{LiAlO}_2$  can suppress structural cracks and inhibit the side reaction with the electrolyte. The cathode material was prepared into a 3.5 Ah soft-pack battery with graphite anode, exhibiting high capacity and excellent cycling performance, with a 20 C fast charging rate capacity of  $127.7 \text{ mAh}\cdot\text{g}^{-1}$ , a retention rate of 97.4% after 100 cycles, and only 5.6% capacity loss after 500 cycles. Manthiram et al. [99] investigated the surface morphology, crystal structure, and electrochemical properties of NMC, NCA, NMA (Al-doped), and NMCAM (Al-Mg co-doped) high-nickel cathode materials with the same nickel content. It was found that  $\text{Al}^{3+}$  can effectively suppress the structural phase transition of high-nickel cathodes and reduce lithium–nickel intermixing and the leaching of transition metal. The performance of NMA, such as rate capability, cycling stability, and thermal stability, is comparable to that of commercialized NMC and NCA, providing a cost-effective cathode material for the development of the next generation of high-performance cobalt-free LIBs. Hou et al. [100] synthesized the Al-doped high-nickel cobalt-free cathode material  $\text{LiNi}_{0.90}\text{Mn}_{0.06}\text{Al}_{0.04}\text{O}_2$  (NMA9064) using the organic amine co-precipitation method and compared it with NC9010 and NMC9064 cathode materials. The results showed that the initial discharge specific capacity of the NMA cathode is  $223.1 \text{ mAh}\cdot\text{g}^{-1}$  (0.1 C, 2.5–4.3 V), which is lower than that of NC9010 and NMC9064, but its average discharge voltage is 47 and 17 mV higher, respectively. The NMA cathode also exhibited a high specific capacity of  $232.1 \text{ mAh}\cdot\text{g}^{-1}$  even at high voltage at 2.5–4.5 V, and the capacity retention rate after 100 cycles at 0.5 C was maintained at 93.3%, higher than that of NC (66.9%). Liu et al. [101] synthesized Al-doped high-nickel cobalt-free single-crystal cathode material  $\text{LiNi}_{0.8}\text{Mn}_{0.16}\text{Al}_{0.04}\text{O}_2$  without cracks by the stirring-assisted cation chelation and recombination route. The discharge specific capacity is  $204 \text{ mAh}\cdot\text{g}^{-1}$  at 0.1 C, and the rate capability is excellent ( $143 \text{ mAh}\cdot\text{g}^{-1}$  at 10 C). The excellent electrochemical performance can be attributed to the synergistic effect of the successful doping of Al elements in the single-crystal structure of the cathode, achieving rapid ion and electron transfer, suppressing Li/Ni mixing, and maintaining structural stability. Li et al. [102] synthesized Gd-doped and  $\text{Gd}_2\text{O}_3$ -coated NCM811 by solid-phase high-temperature synthesis. Due to the high bond dissociation energy ( $716 \text{ kJ}\cdot\text{mol}^{-1}$ ) of Gd–O and the uniform coating of  $\text{Gd}_2\text{O}_3$ , the structural stability and electrochemical performance of NCM can be effectively improved. The capacity retention rate after 100 cycles (3.0–4.4 V, 1 C) was improved by 11% compared to the original NCM.

The doping elements, such as  $\text{Zr}^{4+}$ ,  $\text{Ti}^{4+}$ , and  $\text{Ge}^{4+}$ , are also commonly used in cathode materials. The ionic radius of  $\text{Zr}^{4+}$  is 0.072 nm, much larger than that of transition metals such as Ni, Co, and Mn. The introduction of Zr can increase the Li migration channel and improve the rate performance and cycling performance of cathode materials. Furthermore, Zr does not participate in the electrochemical process and therefore can effectively reduce the local collapse of the crystal structure during charge–discharge processes. Li et al. [107] synthesized Zr-doped Ni–Al-based high-nickel and cobalt-free cathode material  $\text{LiNi}_{0.9}\text{Al}_{0.1-x}\text{Zr}_x\text{O}_2$  (NAZ) using the sol-gel method. The NAZ showed good crystal structure stability and electrochemical performance. The initial discharge capacity was

177.5 mAh·g<sup>-1</sup>, with a capacity retention of 92.45% after 100 cycles. Lai et al. [110] synthesized high-voltage single-crystal cathode material LiNi<sub>0.6</sub>Co<sub>0.1</sub>Mn<sub>0.3</sub>O<sub>2</sub> (Z/T@SC-NCM) with in situ doping of Zr and Ti by precursor co-precipitation. Both experimental analysis and theoretical calculations revealed the synergistic effect of Zr/Ti co-doping on the transition metal (TM) sites in the SC-NCM material, which not only effectively improved the diffusion migration rate of Li<sup>+</sup> but also reduced the stress concentration and cation disorder inside particles. The capacity retention rate of its soft-packed full battery was 80.6% after 4000 cycles, which can meet the lifespan requirements of new energy electric vehicles for more than 10 years. Li et al. [111] synthesized high-nickel and cobalt-free cathode material LiNi<sub>0.9</sub>Mn<sub>0.1</sub>O<sub>2</sub> (NMGe) with lattice in situ doping of Ge and interface coating of Li<sub>4</sub>GeO<sub>4</sub>. The non-magnetic Ge<sup>4+</sup> doping in the transition metal layer effectively reduced the magnetic resistance and lattice oxygen loss and reduced cation mixing and gas evolution. The coating of superionic conductive and corrosion-resistant Li<sub>4</sub>GeO<sub>4</sub> enhanced the surface chemical stability and Li ion migration interface kinetics. The discharge capacity of NMGe at 0.1 C and 10 C was 223.3 and 127.5 mAh·g<sup>-1</sup>, respectively. The capacity retention rate after 500 cycles at 3 C in soft-packaged batteries can be maintained at 80.5%.

The metal elements doped with higher valence Nb<sup>5+</sup>, Ta<sup>5+</sup>, Mo<sup>6+</sup>, and W<sup>6+</sup> and lower valence Mg<sup>2+</sup>, Ca<sup>2+</sup>, Sr<sup>2+</sup>, Zn<sup>2+</sup>, Na<sup>+</sup>, etc., are similar to the previous doping mechanism. Xiao et al. [116] synthesized LiNi<sub>0.83</sub>Co<sub>0.11</sub>Mn<sub>0.06</sub>O<sub>2</sub> cathode material doped with Nb<sub>2</sub>O<sub>5</sub>. The GSAS software refinement results indicate that the Nb<sup>5+</sup>-doped sample possesses a perfect crystal structure, a wider Li<sup>+</sup> diffusion path, and excellent electrochemical properties. Even after 200 cycles at a high temperature of 60 °C with a 1 C rate, the capacity retention can be maintained at 71.7%. Sun et al. [119] conducted a systematic study of the effects of Mg<sup>2+</sup>, Al<sup>3+</sup>, Ti<sup>4+</sup>, Ta<sup>5+</sup>, and Mo<sup>6+</sup> doping elements on the internal structure, electrochemistry, morphology, and chemical properties of LiNi<sub>0.91</sub>Co<sub>0.09</sub>O<sub>2</sub> (NC90). The data from cross-sectional SEM, HPPC, crystal structure analysis, and soft-pack full-cell cycles demonstrated that the cathode material synthesized with high-oxidation-state dopants can relieve the microcracks after charging and discharging cycles, resulting in better cycling performance. Specifically, the cathode materials doped with Ta<sup>5+</sup> and Mo<sup>6+</sup> retain 81.5% of their capacity after 3000 cycles. Park et al. [123] also systematically studied the effects of Co<sup>3+</sup>, Al<sup>3+</sup>, Ti<sup>4+</sup>, Nb<sup>5+</sup>, Ta<sup>5+</sup>, W<sup>6+</sup>, and Mo<sup>6+</sup> doping on the performance of the high-nickel cobalt-free cathode material LiNi<sub>0.9</sub>Mn<sub>0.1</sub>O<sub>2</sub> (NM90). The study showed that Mo doping can eliminate the harmful strain caused by lattice contraction, reduce the formation of microcracks inside particles (Figure 5c,d), and improve structural stability (Figure 5e). Xiao et al. [127] investigated the effect of W doping on the performance of LiNi<sub>0.83</sub>Co<sub>0.11</sub>Mn<sub>0.06</sub>O<sub>2</sub>. It was found that W doping can suppress the anisotropic volume changes caused by the repeating the H2-H3 phase transition, prevent the formation of particle microcracks, and inhibit side reactions. The cathode material doped with W exhibited a discharge capacity of 190.6 mAh·g<sup>-1</sup> at 0.1 C, and the capacity retention rate remains at 69.9% after 500 cycles at 2 C.

Doping with non-metallic element B is also a common method of modifying high-nickel cathode materials. The introduction of high-bond-energy B-O covalent bonds can inhibit the change of 2p orbitals of oxygen atoms and the formation of particle microcracks during cycling. Sun et al. [145] studied the effect of B doping on the microstructure of NCA. The study found that B doping can reduce the surface energy of the (003) crystal plane, promote the preferential growth of the (003) crystal plane, and change the microstructure. LiNi<sub>0.878</sub>Co<sub>0.097</sub>Al<sub>0.015</sub>B<sub>0.01</sub>O<sub>2</sub> cathode material can maintain 83% of its capacity retention after 1000 cycles at a discharge depth of 100%, while the normal undoped LiNi<sub>0.885</sub>Co<sub>0.1</sub>Al<sub>0.015</sub>O<sub>2</sub> showed a capacity retention rate of 49%. The excellent cycling performance indicated that B doping can effectively control microstructures such as particle size and crystal growth orientation, ultimately improving the structural stability and cycling performance. Qu et al. [146] studied the effect of B doping on the structural stability, particle microcracks, and electrochemical performance of LiNi<sub>0.83</sub>Co<sub>0.05</sub>Mn<sub>0.12</sub>O<sub>2</sub>. The results showed that B doping in the TM layer would help to form stronger B-O covalent bonds

and increase the layer spacing, enhancing the thermodynamics and kinetics of cathodes. As a result of the synergistic effect of single-crystal structure and appropriate B doping, the occurrence of internal strain and structural degradation can be effectively alleviated. Even under harsh conditions of high temperature and high cut-off voltage, the cathode doped with 0.6 mol% B showed enhanced rate capability and excellent cycling stability. The retention after 500 cycles in the soft-pack full cell can reach 91.35%, and the capacity decay per cycle was only 0.0173%.

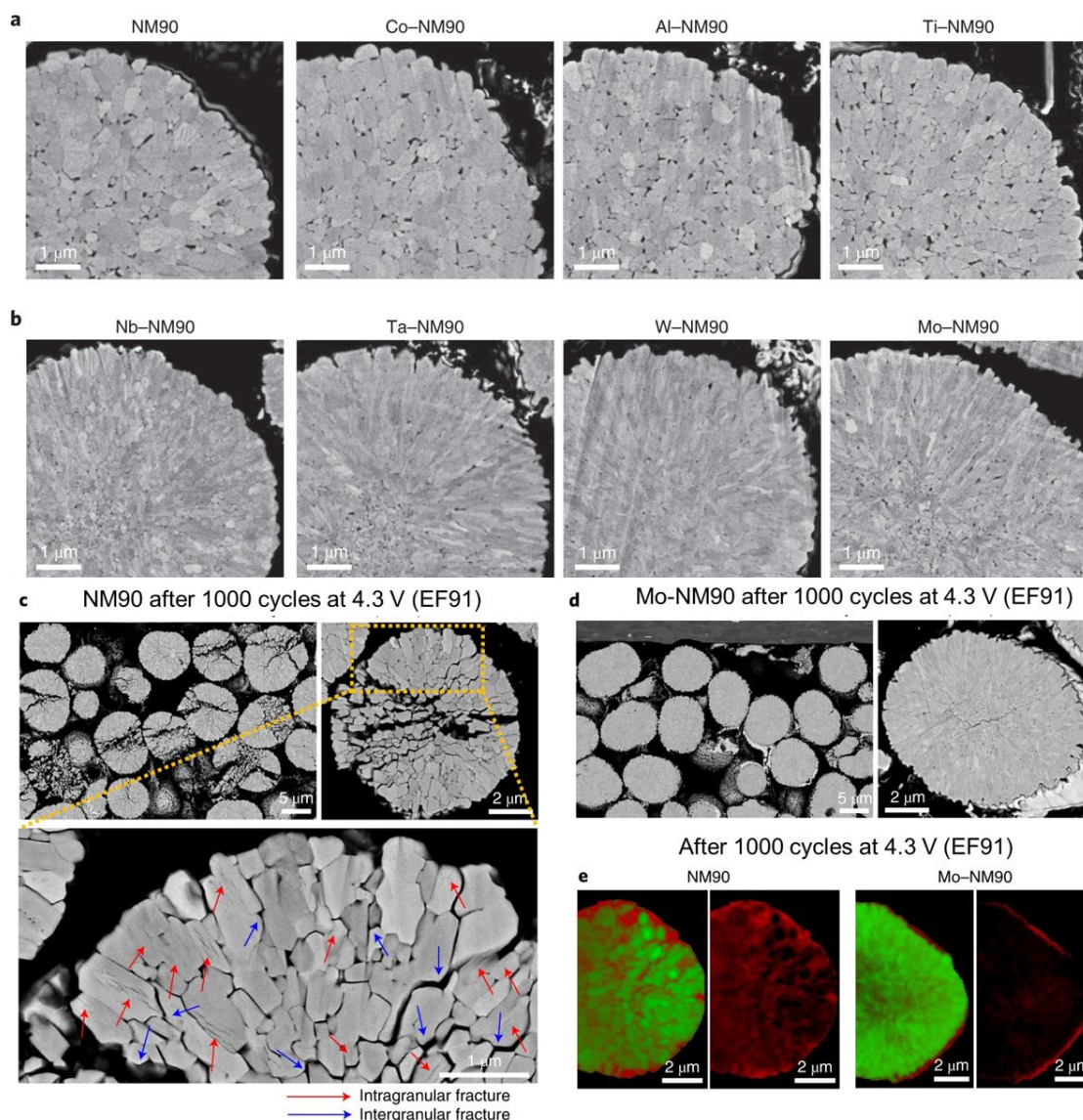


**Figure 5.** Cross-sectional SEM comparison of primary particle morphology of NM90 undoped and doped cathode materials: (a) NM90, Co-NM90, Al-NM90, and Ti-NM90; (b) Nb-NM90, Ta-NM90, W-NM90, and Mo-NM90. NM90 undoped and doped cathode materials cross-sectional SEM and EDS comparison after 1000 cycles of full-cell cycling: cross-sectional SEM of NM90 (c) and Mo-NM90 (d); (e) chemical phase diagrams of NM90 and Mo-NM90 cathode particles in cross-section after 1000 cycles of complete discharge in a full cell with EF91 electrolyte (red and green colors indicate Ni<sup>2+</sup> and Ni<sup>3+</sup>, respectively). Reproduced with permission [123]. Copyright (2022) Nature.

The halogen F is a commonly used doped anionic element. F doping can reduce charge transfer resistance, lower the impedance of cathode materials, reduce HF corrosion, and improve structural stability and cycling performance. Li et al. [147] studied the effect of F-doping substitution on the structure, morphology, and electrochemical properties of

NCM811. XRD, compositional analysis, and XPS characterizations confirmed the incorporation of F into the particles of cathode material. The initial discharge capacity was slightly lower than undoped NCM811, but the cycling performance was greatly improved, especially the high-temperature cycling performance. The performance of anion F and cation co-doping is better than that of single-element doping [152,153]. Yoon et al. [154] studied  $\text{LiNi}_{0.885}\text{Co}_{0.100}\text{Al}_{0.015}\text{O}_2$  (NCA89) co-doped with Ga and B. The study found that the initial discharge capacity of the NCA89 cathode material doped with 0.25 mol% B and 0.75 mol% Ga was  $222.2 \text{ mAh}\cdot\text{g}^{-1}$ , and the capacity retention rate after 100 cycles was 91.7%. The capacity retention rate of the original NCA89 was only 79.4% of its initial capacity. Research data demonstrated that the synergistic effect of multiple doping can effectively stabilize the structural stability of high-nickel cathode materials and improve battery cycling performance.

#### 4.3. Interfacial Modification by Surface Coating

The surface of high-nickel cathode materials tends to form surface residual alkalis, such as LiOH and  $\text{Li}_2\text{CO}_3$ , which can affect the processing of battery slurry. In addition, surface residual alkalis can reduce the electron conductivity and ion diffusion rate of the cathode materials, leading to performance degradation, such as an increase in battery impedance and a decrease in rate capability. During the charge and discharge process, residual alkalis, such as LiOH and  $\text{Li}_2\text{CO}_3$ , can react with trace amounts of moisture in the electrolyte to form HF, which can corrode the battery electrode, causing a rapid decline in cycle capacity, gas production, and other serious issues. The current industrial production of high-nickel cathode materials commonly involves washing the surface residual alkalis with water. During the washing process, a  $\text{Li}^+/\text{H}^+$  ion exchange reaction occurs, causing the surface and near-surface regions of the particles to lose lithium. The proton migration inward leads to a contraction of the layered crystal structure of the cathode material perpendicular to the transition metal layer and O oxygen layer. Meanwhile, Li migration outward leads to a decrease in the electrochemical activity of Li in high-nickel cathode materials, which in turn reduces their capacity, cycle, high-temperature, safety, and other performance. Surface coating is a common modification method for high-nickel cathode materials, which can reduce surface residual alkalis or convert them into fast ion conductors, increase the diffusion rate of Li ion diffusion, and slow down the side reactions and phase transitions between the cathode material surface and the electrolyte during cycling. Through surface coating modification, the surface structure of high-nickel cathode materials can be stabilized, the dissolution of transition metals such as Ni, Co, and Mn can be reduced, the structural stability and conductivity of the cathode materials can be improved, and microcracks and particle pulverization can be reduced, thereby improving the performance of the cathode.

The surface coating of high-nickel cathode materials mainly includes metal oxides, metal fluorides, metal phosphates, lithium-containing compounds, and non-metallic compounds. Metal oxide surface coatings mainly include  $\text{SiO}_2$  [158–160],  $\text{ZrO}_2$  [161],  $\text{TiO}_2$  [162–164],  $\text{Al}_2\text{O}_3$  [165],  $\text{Ta}_2\text{O}_5$  [166], Al+Ti [167], Al+W [168], Co+Ti [169], Co+B [170], Co+Al [171], La+Ca [172], etc. Sun et al. [163] prepared spherical high-nickel cathode material  $\text{LiNi}_{0.9}\text{Co}_{0.08}\text{Al}_{0.02}\text{O}_2$  with 0.4 wt%  $\text{TiO}_2$  coating using the immersion-hydrolysis method. SEM, HRTEM, and XRD results show that  $\text{TiO}_2$  is uniformly coated on the surface of  $\text{LiNi}_{0.9}\text{Co}_{0.08}\text{Al}_{0.02}\text{O}_2$  particles. The capacity retention rate of the cell prepared with coated  $\text{LiNi}_{0.9}\text{Co}_{0.08}\text{Al}_{0.02}\text{O}_2$  after 100 cycles at 2 C rate was 77.0%, which was significantly higher than that of the uncoated NCA (63.3%). The results indicated that the coating can inhibit the oxidative side reaction between the particle surface and the electrolyte, improving the structural stability and cycling performance. Liu and colleagues [166] employed a one-step high-temperature solid-state sintering method to synthesize  $\text{LiNi}_{0.8}\text{Co}_{0.15}\text{Al}_{0.05}\text{O}_2$  material with dual modification of Ta doping and Ta coating (NCA- $\text{Ta}_2\text{O}_5$ ). The  $\text{Ta}_2\text{O}_5$  protective coating can suppress the side reactions between the electrode material and the electrolyte, and the  $\text{Ta}^{5+}$  doping can reduce the  $\text{Li}^+/\text{Ni}^{2+}$  mixing. The obtained NCA- $\text{Ta}_2\text{O}_5$  exhibited an excellent capacity retention rate of 94.46% after 200 cycles at a 1 C rate, which

was significantly higher than the original NCA material at 60.97%. Structural analysis showed that NCA-Ta<sub>2</sub>O<sub>5</sub> maintained a good spherical structure without obvious cracks after 200 cycles at 1 C, while the original NCA experienced severe structural collapse. Wang and colleagues [167] synthesized NCM811 with Al and W coatings. The coated NCM811 exhibited excellent electrochemical stability and safety, and the capacity retention rates after 100 cycles at 25 °C and 60 °C were improved by 13.8% and 25.4%, respectively. Differential scanning calorimetry analysis showed a 50.6% and 45.3% reduction in released heat, and the peak temperature of the exothermic peak increases from 206.1 °C to 223.8 °C, respectively. Coating NCM811 with both Al and W can improve cycling and thermal stability. Huang et al. [168] synthesized Ti-doped and Co-coated high-nickel cathode material T1Co0.5-NCM, which showed improved cycling stability. Ti-doping effectively reduced cation mixing and stabilized the crystal structure. In addition, the spinel phase formed on the surface by Co oxide coating was more stable than the layered phase under high pressure, which can reduce microcrack formation. The material showed a capacity retention of 74.2% after 400 cycles, significantly higher than that of the original cathode (59.5%). Cho et al. [169] synthesized B-coated NCM811 using a coating and injection strategy. Atomistic simulation identified the critical role of strong selective interfacial bonding in uniform reaction wetting, reducing surface/interface oxygen activity and promoting excellent mechanical and electrochemical stability of the injected electrode. The full surface coverage of secondary particles and injection into grain boundaries suppressed microstructure degradation and side reactions with the electrolyte, leading to reduced microcracks after cycling (Figure 6). Yang et al. [170] synthesized LiNi<sub>0.8</sub>Co<sub>0.15</sub>Al<sub>0.05</sub>O<sub>2</sub> using Co+Al layered double hydroxide (LDH) nano-coating on a Ni(OH)<sub>2</sub> precursor. The Co+Al-LDH coating reacted with LiOH and annealed to form an intermediate phase Li<sub>1-x</sub>(Co<sub>0.75</sub>Al<sub>0.25</sub>)<sub>1+x</sub>O<sub>2</sub> as a buffer layer, which improved the layered structure and reduced Li<sup>+</sup>/Ni<sup>2+</sup> cation mixing, forming an ordered and stable crystal structure. Spectroscopic analysis and density functional theory calculations showed a synergistic diffusion effect between Co and Al, and the presence of Co on the surface promoted the diffusion of Al during lithiation and annealing, avoiding the formation of unwanted Al-related impurities and promoting uniform element distribution.

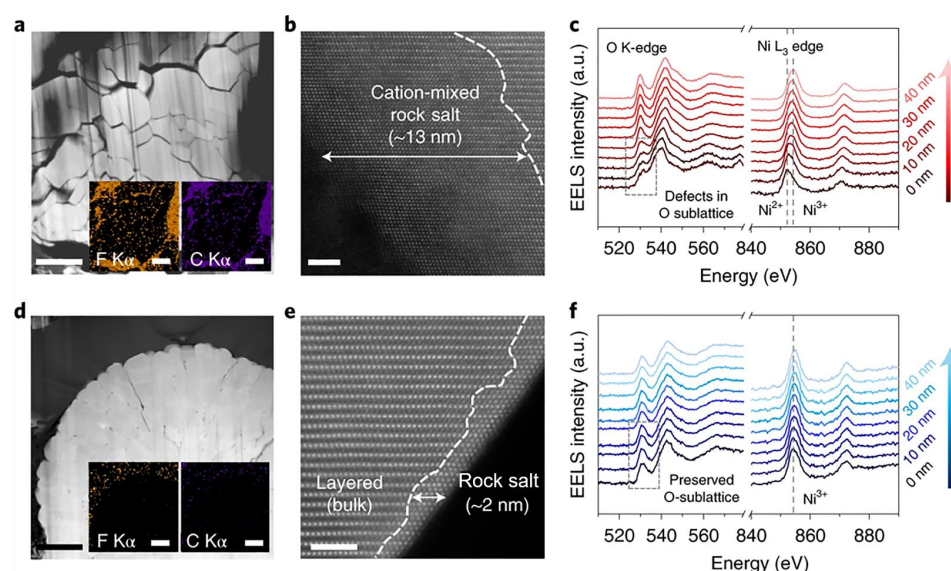


**Figure 6.** (a) TEM and EDS images of pristine NCM after 200 cycles at 45 °C and 7 C. (b) High-resolution transmission electron microscopy (HR-TEM) on a fresh surface produced by intergranular cracking. (c) EELS line scan on the surface of secondary particles in cycled pristine NCM. (d) TEM image and EDS mapping of CoxB-NCM after 200 cycles at 45 °C and 7 C. (e) HR-TEM image of CoxB-NCM. (f) EELS line scan. Reproduced with permission [169]. Copyright (2021) Nature.

The metal fluorides that are suitable for surface coating include LiF [173], AlF [174,175], etc. Coating fluoride on cathode materials can reduce charge transfer resistance and improve rate capability and cycle life. Li et al. [173] confirmed through various tests, such as XRD, TEM, EDX, and XPS, that the residual lithium salt on the surface of NCM811 can react with ammonium fluoride in situ to form a LiF coating. The LiF can improve the discharge rate capability and cycling performance of high-nickel cathode materials. After modification, the capacity loss after 200 cycles was 17.8%, which was greatly improved compared to the capacity loss of 28.2% without modification. Coating with metal phosphates is also a more common modification method for cathode materials, including  $\text{Co}_3(\text{PO}_4)_2$  [176],  $\text{Ni}_3(\text{PO}_4)_2$  [177],  $\text{Mn}_3(\text{PO}_4)_2$  [178],  $\text{FePO}_4$  [179],  $\text{AlPO}_4$  [180],  $\text{Y}(\text{PO}_3)_3$  [181],  $\text{CeP}_2\text{O}_7$  [182],  $\text{LaPO}_4$  [183], etc. Liu et al. [179] designed and prepared  $\text{Y}(\text{PO}_3)_3$ -coated  $\text{LiNi}_{0.8}\text{Co}_{0.15}\text{Al}_{0.05}\text{O}_2$  to reduce the surface residual alkali and improve the gas generation problem of cathode materials. The in situ-formed composite lithium-ion conductor coating ( $\text{Y}(\text{PO}_2)_3\text{-Li}_3\text{PO}_4\text{-YPO}_4$ ) also improved electrochemical behavior. The electrode modified with 2 mol%  $\text{Y}(\text{PO}_3)_3$  showed excellent rate performance ( $156.3 \text{ mAh}\cdot\text{g}^{-1}$  at 5 C) and cycling stability with a capacity retention of 88.3% after 200 cycles. Even at a high temperature of 55 °C, the electrode modified with 2 mol%  $\text{Y}(\text{PO}_3)_3$  still maintained a high reversible capacity, with a capacity retention rate of 89.4% after 100 cycles. Cao et al. [182] synthesized  $\text{CeP}_2\text{O}_7$ -coated high-nickel cathode  $\text{LiNi}_{0.83}\text{Co}_{0.12}\text{Mn}_{0.05}\text{O}_2$  through a PEG-assisted water deposition method. The coating material has good interface stability and can inhibit structural degradation, improving the thermal stability and rate performance of the cathode material. After coating modification, the material maintained a retention rate of 92.38% after 100 cycles under the conditions of 2 C and 4.3 V upper cut-off voltage. Liu et al. [183] introduced a  $\text{LaPO}_4$  coating on the surface of  $\text{LiNi}_{0.87}\text{Co}_{0.09}\text{Al}_{0.04}\text{O}_2$  through a wet coating method and doped a small amount of  $\text{La}^{3+}$  on the surface to achieve dual functions of coating and doping. The sample modified with 2 wt%  $\text{LaPO}_4$  (L2-NCA) had the best electrochemical performance, with capacity retention rates of 96.0% and 85.1% after 100 cycles at 25 °C and 60 °C, respectively, showing better cycling stability than the original NCA with capacity retention rates of 87.1% and 74.2%, respectively.

Metal oxide, fluoride, and phosphate coatings are relatively stable and can reduce the side reactions between the high-nickel cathode material and the electrolyte. However, they can increase the corresponding charge transfer resistance. To solve this issue, researchers have introduced lithium-containing compounds with high  $\text{Li}^+$  conductivity for surface modification. These compounds include  $\text{LiCoO}_2$  [184],  $\text{LiNi}_{0.333}\text{Co}_{0.333}\text{Mn}_{0.333}\text{O}_2$  [185],  $\text{Li}_2\text{ZrO}_3$  [186–188],  $\text{LiZr}_2(\text{PO}_4)_3$  [189],  $\text{LiAlO}_2$  [190],  $\text{Li}_2\text{SiO}_3$  [191],  $\text{Li}_2\text{MnO}_3$  [192],  $\text{LiNbO}_3$  [193,194],  $\text{LiFePO}_4$  [195,196],  $\text{Li}_3\text{PO}_4$  [197–199],  $\text{LiH}_2\text{PO}_4$  [200],  $\text{LiBO}$  [201,202], and LLAO [203]. Yang et al. [188] utilized the Couette–Taylor reaction to deposit a surface-coated  $\text{Li}_2\text{ZrO}_3$  layer onto  $\text{LiNi}_{0.90}\text{Co}_{0.04}\text{Mn}_{0.03}\text{Al}_{0.03}\text{O}_2$  (NCMA), with a thickness of approximately 2.5 nm. Electrochemical impedance spectroscopy (EIS), cyclic voltammetry (CV), and the galvanostatic intermittent titration technique (GITT) demonstrated that the coating acted as a bridge, lowering activation energy and polarization potential, thereby facilitating the transport of Li ions. After 100 cycles at 1 C, the capacity retention rate of the cathode material coated with 1 wt% of the layer was 90.2% (bare NCMA was 74.6%). The data confirmed that the  $\text{Li}_2\text{ZrO}_3$  coating can enhance the structural stability and cycling performance of the cathode. Li et al. [191] synthesized NCM811 coated with  $\text{Li}_2\text{SiO}_3$ . The coating resulted in a marked reduction in the occurrence of microcracks on the particle surface, demonstrating improved structural stability and cycling performance. Zhao et al. [192] synthesized NCM811 coated with  $\text{Li}_2\text{MnO}_3$  (LMO). The LMO coating effectively suppressed harmful structural degradation of the high-nickel cathode, improving cycling stability. The optimized NCM811@LMO-3% cathode material exhibited a capacity retention rate of approximately 93% after 100 cycles at 0.1C and a capacity retention rate of 81% at 1 C after 500 cycles, better than bare NCM811 materials (74% and 63%). Zhang et al. [194] prepared  $\text{LiNbO}_3$ -coated single-crystal NCM811. Molecular dynamics simulations confirmed that the  $\text{LiNbO}_3$  coating effectively inhibited the dissolution of transition metals

while providing a stable Li ion pathway. Experimental results also showed that coating modification effectively improved the cycling stability of NCM811, increasing the capacity retention rate from 19% to 70% after 500 cycles. Zhang et al. [196] introduced a modification strategy of Mg doping and  $\text{LiFePO}_4$  coating on NCM811. The modified cathode displayed lower charge transfer resistance than the original material. Liu et al. [200] synthesized NCA with a surface-coated  $\text{LiH}_2\text{PO}_4$  layer by converting the surface residue to  $\text{LiH}_2\text{PO}_4$ . The coated NCA exhibited a significantly improved cycling retention rate of 96.1% and 90.5% at 25 °C and 55 °C, respectively. Wang et al. [202] prepared  $\text{LiNi}_{0.90}\text{Co}_{0.06}\text{Mn}_{0.04}\text{O}_2$  coated with LBO via a dry process. The coating reduced the direct contact between the cathode material and the electrolyte, suppressing structural degradation and surface impedance. The material had a discharge capacity of  $222.0 \text{ mAh}\cdot\text{g}^{-1}$ . The capacity retention rate after 100 cycles at 1 C was 88.1%. He et al. [203] developed a modified  $\text{LiNi}_{0.82}\text{Co}_{0.14}\text{Al}_{0.04}\text{O}_2$  cathode material by applying an in situ coating of  $\text{Li}_{0.5}\text{La}_2\text{Al}_{0.5}\text{O}_4$  (LLAO) and doping it with Mn for compensation. This modification technique effectively reduced the  $\text{Li}^+/\text{Ni}^+$  disorder and microcracks in secondary particles, thereby improving the material's mechanical properties. The modified material showed an impressive 96.2% capacity retention after 100 cycles at a voltage range of 3.0–4.4 V and a rate of 1 C, representing a 13% enhancement compared to the original material.

Non-metallic compound coating mainly involves B-containing compounds [204–206] and polymers [207,208]. B-containing compounds, such as boron oxide or boric acid, can react with the residual alkali on the surface of cathode materials to form fast ionic conductor compound LBO, which can reduce microcracks in high-nickel cathode materials and improve their capacity and cycling performance. Kim et al. [205] prepared a fast ionic conductor  $\text{Li}_3\text{BO}_3$  coating and B-doped co-modified  $\text{LiNi}_{0.91}\text{Co}_{0.06}\text{Mn}_{0.03}\text{O}_2$ . It was confirmed by XPS, FESEM, and FETEM that the microcracks of the modified material were greatly alleviated. The discharge capacity of the modified  $\text{LiNi}_{0.91}\text{Co}_{0.06}\text{Mn}_{0.03}\text{O}_2$  (LBO-0.05) at 5 C rate was  $88.6 \text{ mAh}\cdot\text{g}^{-1}$ , which was greatly improved compared to the  $45.8 \text{ mAh}\cdot\text{g}^{-1}$  of original NCM. Cao et al. [206] introduced a dual-modified coating of  $\text{B}_2\text{O}_3$  and  $\text{LiBO}_2$  to the high-nickel material  $\text{LiNi}_{0.89}\text{Co}_{0.08}\text{Mn}_{0.03}\text{O}_2$  (NCM89). The research results showed that the modification strategy can inhibit the dissolution of transition metals and the decomposition of the electrolyte at the cathode/electrolyte interface, producing a beneficial cathode–electrolyte interface layer (CEI). The discharge capacity of the cathode was  $180.4 \text{ mAh}\cdot\text{g}^{-1}$ , and the capacity retention rate after 100 cycles at 1 C was 90%, which was significantly higher than the 59% of the original cathode. Kim et al. [207] conducted surface modification of NCM622 by introducing a dual-conductive polymer coating of poly(3,4-ethylenedioxythiophene)-co-poly(ethylene glycol) (PEDOT-co-PEG). The conductive polymer coating inhibited the growth of the surface resistance layer of the cathode material and suppressed the dissolution of transition metals from the active cathode material. The modified material exhibited significantly improved discharge capacity, high-rate performance, and high-temperature performance. Hwang et al. [208] synthesized a lithium-containing “BTJ-L” hybrid oligomer coating of NCM811 by using a bismaleimide (BMI) with a polyether monoamine (JA), thiocyanic acid (TCA), and LiOH. The electrochemical performance of the material, such as discharge capacity, Coulombic efficiency, and cycling retention rate, was greatly improved.

#### 4.4. Optimal Regulation of Crystal Structure

The grains of high-nickel polycrystalline cathode material are formed by the aggregation of multiple primary particles. Therefore, cracks and large gaps between particles are prone to occur during the compaction process of electrode sheets. The poor structural stability of the high-nickel polycrystalline cathode may bring many issues, such as surface microcracks, particle fragmentation, rapid cycle life decay, poor thermal stability, and safety hazards during the charge and discharge process. Single-crystal cathode material is composed of one or more large particles of single-crystal shape. Due to the smooth surface, high density, and mechanical strength of single-crystal particles and the absence of grain

boundaries inside, they are not easily reacted with the electrolyte to cause microcracks and structural phase transitions, thus improving the structural stability and cycling performance of the high-nickel cathode [209–218]. Therefore, single crystallization is one of the important paths to ensure that high-nickel cathode materials have both high energy density and long cycling stability.

Xiao et al. [219] studied the gas evolution mechanism of single-crystal and polycrystalline cathode materials of  $\text{LiNi}_{0.76}\text{Mn}_{0.14}\text{Co}_{0.1}\text{O}_2$  (NMC76) by using button cells and soft-packaged cells. The study found that single-crystal materials generally require higher electrochemical driving forces to produce gas. The gas evolution of single-crystal materials is much lower than that of polycrystalline materials even at high voltage potentials, indicating that the low gas evolution of single-crystal materials is one of the important paths to solve the safety issues of high-nickel batteries. Battaglia et al. [220] studied the full battery performance of single-crystal and polycrystalline cathode materials of NCM622. The study found no significant difference in the thickness of the cation-disordered layer formed in the surface region of the cathode particles between single-crystal and polycrystalline particles. However, the cracking phenomenon of polycrystalline particles was marked, while single-crystal particles showed almost no cracking phenomenon, and the corresponding gas evolution was also lower. Sun and Yoon [221] demonstrated that single crystals (NCM) can effectively address the issue of microcracks in cathode particles. The study found that the single-crystal  $\text{LiNi}_{0.7}\text{Co}_{0.15}\text{Mn}_{0.15}\text{O}_2$  (SC-NCM70) did not undergo irreversible structural damage even when charged to 4.3 V. However, when the Ni content was increased to 90%, microcracks were observed in both the SC-NCM90 particles and their phase boundaries (Figure 7), indicating that a Ni content greater than 90% may be a bottleneck in improving the energy density and cycling performance of high-nickel single-crystal materials. Their further research found that reducing the charging rate of single-crystal materials with Ni > 90% or reducing the size of cathode particles could reduce the occurrence of structural defects at the end of charging, thus improving the structural stability and cycling performance. Zhao et al. [222] prepared high-nickel cobalt-free polycrystalline  $\text{LiNi}_{0.9}\text{Mn}_{0.1}\text{O}_2$  (PC-NM91) and single-crystal  $\text{LiNi}_{0.9}\text{Mn}_{0.1}\text{O}_2$  (SC-NM91) cathodes. They found that the SC-NM91 had lower  $\text{Li}^+/\text{Ni}^{2+}$  mixing and a faster Li ion diffusion rate, which suppressed intergranular cracking, surface pulverization, disorder phase transition, and interfacial side reactions. After 300 cycles at 1 C, the capacity retention of the single-crystal cathode was 85.3%, while that of the polycrystalline PC-NM91 under the same conditions was only 65.8%. Chen et al. [223] combined the high-nickel single-crystal/polycrystalline cathode NMC811 with the solid-state electrolyte  $\text{Li}_3\text{YCl}_6$  and a Li-In alloy anode to form high-energy-density all-solid-state batteries. The study found that the capacity retention of the single-crystal cathode after 1000 cycles at 0.2 C rate was close to 90%. Zhou et al. [224] used the pulse high-temperature sintering (PHTS) strategy to synthesize the high-nickel single-crystal cathode material  $\text{LiNi}_{0.9}\text{Co}_{0.05}\text{Mn}_{0.05}\text{O}_2$  by ultra-short time sintering at 1040 °C. The initial discharge capacity of the material was 209  $\text{mAh}\cdot\text{g}^{-1}$ . The tap density was increased by 1/3 to 2.76  $\text{g}\cdot\text{cm}^{-3}$  compared to polycrystalline. The particle microcracking was successfully suppressed, thus improving the cycling performance and thermal stability of the cathode.

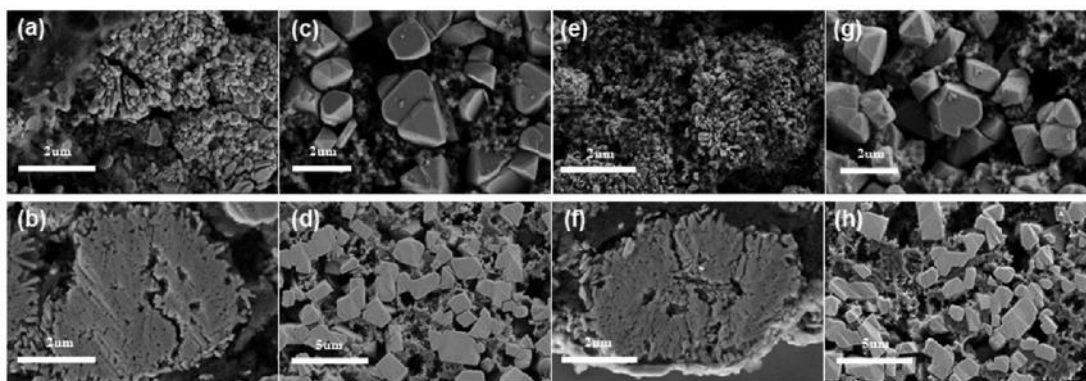


**Figure 7.** SEM and cross-section SEM on the cathode side after 200 cycles under 4.5 V of (a,b) PC-NM91 and (c,d) SC-NM91 and under 2 C of (e,f) PC-NM91 and (g,h) SC-NM91. Reproduced with permission [221]. Copyright (2022) American Chemical Society.

#### 4.5. Designing Composite Structures

High-nickel multi-element cathode materials suffer from poor structural stability, surface microcracking and particle fragmentation, rapid cycle life decay, poor thermal stability, and poor safety performance. In recent years, researchers have addressed the challenge of balancing high capacity and long cycle stability by designing composite structures, such as core–shell structures [225–236] and concentration gradients [237–242]. Chen et al. [225] synthesized a  $\text{Li}(\text{Ni}_{0.8}\text{Co}_{0.1}\text{Mn}_{0.1})_{0.8}(\text{Ni}_{0.5}\text{Mn}_{0.5})_{0.2}\text{O}_2$  composite cathode with a  $\text{LiNi}_{0.8}\text{Co}_{0.1}\text{Mn}_{0.1}\text{O}_2$  core and a  $\text{Li}(\text{Li}_{0.5}\text{Mn}_{0.5})\text{O}_2$  shell. The core material provided high capacity, while the shell material achieved high thermal stability. Sun et al. [228] designed a gradient core–shell  $\text{LiNi}_{0.83}\text{Co}_{0.07}\text{Mn}_{0.10}\text{O}_2$  high-nickel cathode material with a higher Ni content. The inner core was composed of high-nickel  $\text{LiNi}_{0.9}\text{Co}_{0.05}\text{Mn}_{0.05}\text{O}_2$ , while the outer layer was composed of low-nickel  $\text{LiNi}_{0.68}\text{Co}_{0.12}\text{Mn}_{0.20}\text{O}_2$ , which exhibited high capacity, rate capability, and long cycling life. Xiao et al. [230] synthesized the core–shell high-nickel cathode material  $\text{NCM811}@x[\text{Li}-\text{Mn}-\text{O}]$  ( $x = 0.01, 0.03, 0.06$ ) with a nickel-rich core and a manganese-rich shell. The material with  $x = 0.03$  exhibited the best rate performance. Additionally, the material with  $x = 0.03$  showed better thermal stability and a capacity retention of 65.1% after 200 cycles. Chen et al. [231] synthesized the gradient cathode material  $\text{LiNi}_{0.6}\text{Co}_{0.2}\text{Mn}_{0.2}\text{O}_2$  (CG-NCM622) with a high-nickel NCM811 core and a high-stability  $\text{LiNi}_{1/3}\text{Co}_{1/3}\text{Mn}_{1/3}\text{O}_2$  shell. Compared with conventional NCM811, CG-NCM622 displayed better structural stability and excellent electrochemical performance. The initial discharge capacity was  $195.6 \text{ mAh}\cdot\text{g}^{-1}$  at 1 C in the voltage range of 2.8–4.6 V, and the capacity retention rate after 100 cycles was 90%. Sun et al. [232] designed a core–shell composite structure for the high-nickel cathode material  $\text{LiNi}_{0.9}\text{Co}_{0.045}\text{Mn}_{0.045}\text{Al}_{0.01}\text{O}_2$ , with  $\text{LiNi}_{0.92}\text{Co}_{0.04}\text{Mn}_{0.03}\text{Al}_{0.01}\text{O}_2$  as the inner core of the high-nickel cathode particle and  $\text{LiNi}_{0.845}\text{Co}_{0.067}\text{Mn}_{0.078}\text{Al}_{0.01}\text{O}_2$  as the surface buffer layer. This composite microstructure allowed for uniform contraction of primary particle stress and created different stress states that transfer to compressive stress inside the cathode particle, which effectively suppressed microcracks from propagating to the outer surface of the particle. This unique microstructure significantly improved the cycling performance of the cathode, with a capacity retention rate of 84.7% after 1500 cycles. Additionally, the core–shell structure cathode exhibited high mechanical stability and fracture toughness. Sun et al. [233] developed a cobalt-free, nickel-rich core and manganese-rich shell  $\text{LiNi}_{0.9}\text{Mn}_{0.1}\text{O}_2$ . The manganese-rich shell can provide effective internal strain dissipation and chemical protection, which eliminates the internal strains caused by charge state inhomogeneity and cathode fracture toughness. The core–shell  $\text{LiNi}_{0.9}\text{Mn}_{0.1}\text{O}_2$  without cobalt showed excellent long-term cycling stability. The capacity retention rate was 78.5% after 2000 cycles at a charging rate of 1 C and a discharge rate of 0.8 C. The capacity retention rate was 79.5% after 1000 cycles at a charging rate of 3 C and a discharge rate of 1 C. Yang et al. [236] designed a high-nickel, cobalt-free core–shell cathode material by surface coating  $\text{WO}_3$  on a precursor material composed of inner core

$\text{Ni}(\text{OH})_2$  and outer shell  $\text{Ni}_x\text{M}_y(\text{OH})_2$  (Figure 8). The  $\text{Li}_x\text{W}_y\text{O}_z$  secondary phase formed on the surface was infiltrated into the secondary particle grain boundary, which can effectively prevent the diffusion of metal elements in the core–shell, reducing the surface side reactions of high-nickel, cobalt-free cathode materials and enhancing the mechanical strength and electrochemical performance of particles.

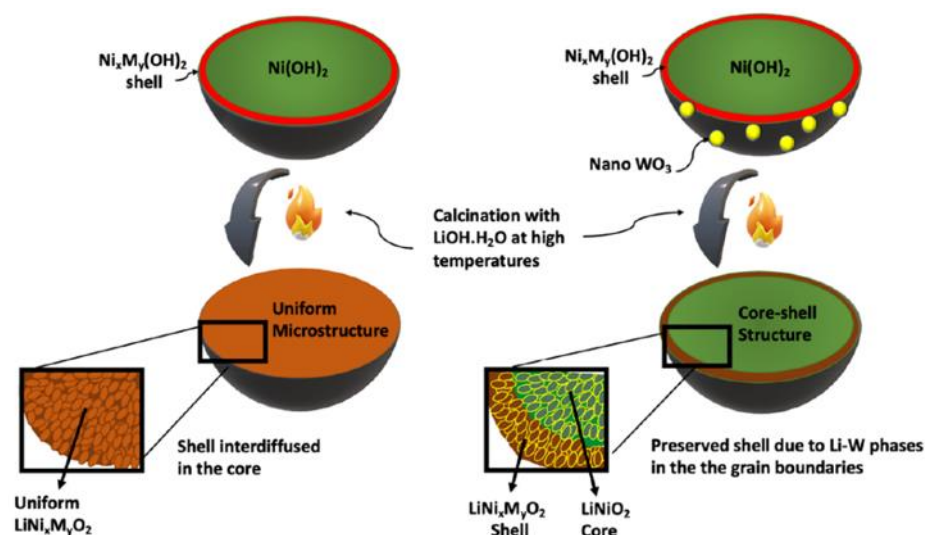


**Figure 8.** Schematic showing the challenge of interdiffusion in core–shell structured particles during synthesis and the preservation of the initial microstructure in  $\text{WO}_3$ -coated precursors after calcination due to the presence of  $\text{Li}_x\text{W}_y\text{O}_z$  phases (shown in yellow) in the grain boundaries. Reproduced with permission [236]. Copyright (2022) American Chemical Society.

Sun et al. [237] designed a gradient material with a high-nickel NCM811 as the core and a low-nickel  $\text{LiNi}_{0.46}\text{Co}_{0.23}\text{Mn}_{0.31}\text{O}_2$  as the shell. The degree of side reactions between the low-nickel cathode material and the electrolyte is smaller than that of the high-nickel cathode material, which is beneficial to reduce the formation of surface microcracks during the cycling process to improve the cycling performance of the cathode. The gradient core–shell high-nickel material can effectively solve the difficulty of Li diffusion caused by the inconsistent contraction of the crystal cell volume between the high-nickel core and the gradient shell and then effectively improve the cycling life of the high-nickel cathode material. In the voltage range of 3.0–4.4V and at a high temperature of 55 °C, the capacity retention rate after 500 cycles at 1 C was 96.5%, which is much higher than the 80.4% of conventional NCM811 materials. Sun et al. [238] synthesized a non-full element gradient cathode material  $\text{LiNi}_{0.60}\text{Co}_{0.15}\text{Mn}_{0.25}\text{O}_2$ , in which the Mn concentration remained constant while the Ni and Co concentrations exhibited a gradient change. The SEM morphology revealed rod-shaped primary particles with radial growth orientation. This non-full element gradient cathode material exhibited significantly improved rate and cycling performance compared to conventional non-gradient materials, with a capacity retention of 70% after 1000 cycles at a high temperature of 55 °C. They also investigated a full element gradient high-nickel cathode material,  $\text{LiNi}_{0.75}\text{Co}_{0.10}\text{Mn}_{0.15}\text{O}_2$  [239]. From SEM and electron probe microanalyzer (EPMA) images, it can be observed that the Mn concentration gradually increased from the inner core of the secondary particles to the outer layer, while the Ni and Co concentrations gradually decreased. The inner core material was composed of high-nickel  $\text{LiNi}_{0.86}\text{Co}_{0.10}\text{Mn}_{0.04}\text{O}_2$ , and the outer layer was composed of low-nickel  $\text{LiNi}_{0.70}\text{Co}_{0.10}\text{Mn}_{0.10}\text{O}_2$ . The precursor morphology of this full gradient concentration material was a primary particle with a rod-shaped morphology and a radial growth orientation, as analyzed by selected area electron diffraction (SAED) and TEM. The initial discharge capacity and rate performance of this material were superior to those of conventional  $\text{LiNi}_{0.86}\text{Co}_{0.10}\text{Mn}_{0.04}\text{O}_2$  cathode materials. Yu et al. [240] synthesized a novel nickel concentration gradient  $\text{LiNi}_{0.8}\text{Co}_{0.15}\text{Al}_{0.05}\text{O}_2$  (NCG-NCA) high-nickel cathode

material. The stable surface structure of NCG-NCA minimized the occurrence of severe atomic rearrangement. The neutron diffraction analysis of NCA revealed that the NCG structure reduced the degree of  $\text{Li}^+/\text{Ni}^{2+}$  mixing, thereby enhancing its cycling stability and rate capability. The NCG-NCA exhibited an outstanding capacity retention of 75% after 200 cycles even at high cutoff voltage of 4.5 V and 10 C rate, which was higher than the 50% of the original NCA (P-NCA) cathode without NCG. Sun et al. [241] compared the discharge capacity, cycling life, high-temperature stability, and particle microcracks of conventional  $\text{LiNi}_{0.90}\text{Co}_{0.05}\text{Mn}_{0.05}\text{O}_2$  (NCM90) and  $\text{LiNi}_{0.90}\text{Co}_{0.045}\text{Mn}_{0.045}\text{Al}_{0.01}\text{O}_2$  (NCMA90) with gradient  $\text{LiNi}_{0.90}\text{Co}_{0.05}\text{Mn}_{0.05}\text{O}_2$  (CSG-NCM90) and  $\text{LiNi}_{0.90}\text{Co}_{0.045}\text{Mn}_{0.045}\text{Al}_{0.01}\text{O}_2$  (CSG-NCMA90) high-nickel cathode materials at different DOD. The research data showed that the microstructure of gradient materials effectively suppressed the formation and expansion of microcracks under high charge states, allowing the CSG-NCMA90 gradient cathode to retain 90.7% of its initial capacity after 1000 cycles at 100% DOD, which is superior to the 60–80% capacity retention rate of traditional nickel-rich layered cathodes. Niu et al. [242] prepared gradient NCM high-nickel cathode materials by modifying the primary and secondary particles of NCM with nickel-based MOF. During the high-temperature sintering process, MOF can form a protective layer of 5–10 nm on the surface of the primary particles, effectively slowing down the occurrence of phase transitions during cycling and suppressing cracks in the particles, thereby effectively improving the cycling stability. In addition, the metal components in MOF can effectively increase the nickel content inside the secondary particles, forming a concentration gradient that gradually increases from the outside to the inside, achieving simultaneous modification of primary and secondary particles. The prepared D-NCM811 exhibited significantly improved cycling stability in both half-cell and full-cell compared to unmodified NMC811. In addition, the D-NCM811 still maintained 84.1% of its initial capacity after 500 cycles at 1 C rate.

## 5. Conclusions

This paper reviews and analyzes the structural characteristics, problems, and recent research progress of high-nickel multifunctional cathode materials and summarizes the progress of performance optimization in terms of precursor growth orientation regulation, bulk phase doping structure regulation, surface coating interface modification, crystal morphology control, and material structure design. In order to achieve the long range and low cost of LIBs, high-nickel multifunctional cathode materials are one of the most promising cathode materials for large-scale industrialization of high-energy-density lithium-ion battery applications. In order to quickly realize the industrial application of high-nickel multifunctional cathode materials, it is also necessary for universities, research institutes, and enterprises to cooperate in production and research. The development and industrialization of high-nickel multicomponent cathode materials should focus on the following aspects:

(1) Increasing research efforts towards low-cobalt ( $\text{Co} < 5 \text{ mol}\%$ ) or cobalt-free high-nickel cathode materials, such as NCM, NCMA, NM, NMA, and NA, to further enhance the high specific energy and low-cost advantages of high-nickel multicomponent cathode materials.

(2) Developing hybrid electrode systems consisting of high-nickel polycrystalline large particles and single-crystal small particles. The crystallization of the high-nickel cathode can improve the battery's cycling and safety performance, meeting the requirements of high voltage and high capacity, long cycle, high-temperature excellence, high safety, low gas generation, and other performance requirements for high-safety long-endurance new energy vehicle power batteries.

(3) Conducting in-depth research on the reaction mechanism, particle stress, morphology, and directional growth control of high-nickel multicomponent precursor synthesis to provide a solid theoretical basis for improving the cycling and safety performance of high-nickel multicomponent cathode materials.

(4) Conducting in-depth analysis of the influence mechanism of modifying methods such as bulk doping and surface coating on the crystal structure, surface stability, particle

strength, and surface microcracks of high-nickel multicomponent cathode materials to further enhance the capacity, cycling, and safety performance of the materials.

(5) Further optimizing the design of high-nickel multicomponent cathode materials with core-shell gradient structure and match them with solid electrolyte systems (LATP/LLTO/LLZO, etc.) to further improve the safety and high-temperature tolerance of batteries.

(6) Developing new processes and equipment with short cycles and high capacity to meet the demands of future large-scale markets and cost reduction, especially for the processing and production of solid-state batteries and all-pole-ear large cylindrical batteries.

(7) The future industrialization direction of high-nickel cathode materials should also focus on ecodesign principles to minimize the environmental impacts of LIBs. This includes considering sustainable sourcing of raw materials, optimizing manufacturing processes, designing batteries with longer lifetimes and easier recyclability, and using environmentally friendly disposal methods. By adopting ecodesign principles, manufacturers can help reduce the environmental impact of high-nickel cathode materials and LIBs, making them a more sustainable energy storage solution.

**Author Contributions:** X.T. and R.G. contributed equally to this work. Conceptualization, X.T. and C.W.; methodology, X.T., C.W., R.G. and J.W.; formal analysis, X.T., R.G. and X.W.; investigation, X.T., R.G., Y.B. and N.L.; writing—original draft preparation, X.T. and R.G.; writing—review and editing, Y.B., X.W., N.L., J.W. and C.W.; supervision, X.W. and C.W.; project administration, Y.B. and J.W.; All authors have read and agreed to the published version of the manuscript.

**Funding:** This work is supported by the National Key Research and Development Program of China (2022YFB2404400), National Natural Science Foundation of China (22075025), Project of Cooperation of the Chinese Academy of Engineering and Local Governments (Grant No. 2021-FJ-ZD-2), the funding from General Research Institute for Nonferrous Metals (C712620213102034), the Science and Technology Program of Guangdong Province (Grant No. 3 2020B0909030004), and the Graduate Interdisciplinary Innovation Project of Yangtze Delta Region Academy of Beijing Institute of Technology (Jiaxing, No. GIIP2022-010).

**Data Availability Statement:** No new data were created or analyzed in this study. Data sharing is not applicable to this article.

**Conflicts of Interest:** The authors declare no conflict of interest.

## References

1. Gao, M.; Li, H.; Xu, L.; Xue, Q.; Wang, X.; Bai, Y.; Wu, C. Lithium metal batteries for high energy density: Fundamental electrochemistry and challenges. *J. Energy Chem.* **2021**, *59*, 666–687. [\[CrossRef\]](#)
2. Zhang, K.; Wu, F.; Zhang, K.; Weng, S.; Wang, X.; Gao, M.; Sun, Y.; Cao, D.; Bai, Y.; Xu, H.; et al. Chlorinated dual-protective layers as interfacial stabilizer for dendrite-free lithium metal anode. *Energy Storage Mater.* **2021**, *41*, 485–494. [\[CrossRef\]](#)
3. Zhao, W.; Zhang, K.; Wu, F.; Wang, X.; Guo, R.; Zhang, K.; Yuan, Y.; Bai, Y.; Wu, C. Moisture-assistant chlorinated separator with dual-protective interface for ultralong-life and high-rate lithium metal batteries. *Chem. Eng. J.* **2023**, *453*, 139348. [\[CrossRef\]](#)
4. Wu, F.; Zhang, K.; Liu, Y.; Gao, H.; Bai, Y.; Wang, X.; Wu, C. Polymer electrolytes and interfaces toward solid-state batteries: Recent advances and prospects. *Energy Storage Mater.* **2020**, *33*, 26–54. [\[CrossRef\]](#)
5. Zhang, K.; Wu, F.; Wang, X.; Zheng, L.; Yang, X.; Zhao, H.; Sun, Y.; Zhao, W.; Bai, Y.; Wu, C. An Ion-dipole-reinforced polyether electrolyte with ion-solvation cages enabling high-voltage-tolerant and ion-conductive solid-state lithium metal batteries. *Adv. Funct. Mater.* **2022**, *32*, 2107764. [\[CrossRef\]](#)
6. Guo, R.; Wu, F.; Wang, X.; Bai, Y.; Wu, C. Multi-electron reaction-boosted high energy density batteries: Material and system innovation. *J. Electrochem.* **2022**, *28*, 2219011.
7. Liu, Z.; Yu, A.; Lee, J.Y. Synthesis and characterization of  $\text{LiNi}_{1-x-y}\text{Co}_x\text{Mn}_y\text{O}_2$  as the cathode materials of secondary lithium batteries. *J. Power Sources* **1999**, *81–82*, 416–419. [\[CrossRef\]](#)
8. Tsutomu, O.; Yoshinari, M. Novel lithium insertion material of  $\text{LiCo}_{1/3}\text{Ni}_{1/3}\text{Mn}_{1/3}\text{O}_2$  for advanced lithium-ion batteries. *Chem. Lett.* **2001**, *30*, 642–643.
9. Zhuang, G.V.; Chen, G.Y.; Shim, J.P.; Song, X.Y.; Ross, P.N. Thomas J Richardson.  $\text{Li}_2\text{CO}_3$  in  $\text{LiNi}_{0.8}\text{Co}_{0.15}\text{Al}_{0.05}\text{O}_2$  cathodes and its effects on capacity and power. *J. Power Sources* **2004**, *134*, 293–297. [\[CrossRef\]](#)
10. Noh, M.-J.; Lee, Y.; Cho, J. Water adsorption and storage characteristics of optimized  $\text{LiCoO}_2$  and  $\text{LiNi}_{1/3}\text{CO}_{1/3}\text{Mn}_{1/3}\text{O}_2$  composite cathode material for Li-ion cells. *J. Electrochem. Soc.* **2006**, *153*, A935–A940.

11. Shizuka, K.; Kiyohara, C.; Shima, K.; Takeda, Y. Effect of CO<sub>2</sub> on layered Li<sub>1+z</sub>Ni<sub>1-x-y</sub>Co<sub>x</sub>M<sub>y</sub>O<sub>2</sub> (M = Al, Mn) cathode materials. *J. Power Sources* **2007**, *166*, 233–238. [[CrossRef](#)]
12. Xiong, X.-H.; Wang, Z.-X.; Yue, P.; Guo, H.-J.; Wu, F.-X.; Wang, J.-X.; Li, X.-H. Washing effects on electrochemical performance and storage characteristics of LiNi<sub>0.8</sub>Co<sub>0.1</sub>Mn<sub>0.1</sub>O<sub>2</sub> as cathode material for lithium-ion batteries. *J. Power Sources* **2013**, *222*, 318–325. [[CrossRef](#)]
13. Xiong, X.-H.; Ding, D.; Bu, Y.; Wang, H.-X.; Huang, B.; Guo, H.-J.; Li, X.-H. Enhanced electrochemical properties of a LiNiO<sub>2</sub>-based cathode material by removing lithium residues with (NH<sub>4</sub>)<sub>2</sub>HPO<sub>4</sub>. *J. Mater. Chem. A* **2014**, *2*, 11691–11696. [[CrossRef](#)]
14. Wu, F.; Tian, J.; Su, Y.-F.; Wang, J.; Zhang, C.-Z.; Bao, L.-Y.; He, T.; Li, J.-H.; Chen, S. Effect of Ni<sup>2+</sup> content on lithium/nickel disorder for Ni-rich cathode materials. *ACS Appl. Mater. Inter.* **2015**, *7*, 7702–7708. [[CrossRef](#)]
15. Xiao, P.; Lv, T.-J.; Chen, X.-P.; Chang, C.-K. LiNi<sub>0.8</sub>Co<sub>0.15</sub>Al<sub>0.05</sub>O<sub>2</sub>: Enhanced electrochemical performance from reduced cationic disordering in Li slab. *Sci. Rep.* **2017**, *7*, 1408–1415. [[CrossRef](#)]
16. Liang, M.; Song, D.-W.; Zhang, H.-Z.; Shi, X.-X.; Wang, Q.; Zhang, L.-Q. Improved performances of LiNi<sub>0.8</sub>Co<sub>0.15</sub>Al<sub>0.05</sub>O<sub>2</sub> material employing NaAlO<sub>2</sub> as a new aluminum source. *ACS Appl. Mater. Inter.* **2017**, *9*, 38567–38574. [[CrossRef](#)]
17. Li, X.; Ge, W.-J.; Wang, H.; Yan, X.-X.; Deng, B.-W.; Chen, T.; Qu, M.-Z. Enhancing cycle stability and storage property of LiNi<sub>0.8</sub>Co<sub>0.15</sub>Al<sub>0.05</sub>O<sub>2</sub> by using fast cooling method. *Electrochim. Acta* **2017**, *227*, 225–234. [[CrossRef](#)]
18. Trease, N.-M.; Seymour, I.-D.; Radin, M.-D.; Liu, H.-D.; Liu, H.; Hy, S.; Chernova, N.; Parikh, P.; Devaraj, A.; Wiaderek, K.-M.; et al. Identifying the distribution of Al<sup>3+</sup> in LiNi<sub>0.8</sub>Co<sub>0.15</sub>Al<sub>0.05</sub>O<sub>2</sub>. *Chem. Mater.* **2016**, *28*, 8170–8180. [[CrossRef](#)]
19. Purwanto, A.; Yudha, C.-S.; Ubaidillah, U.; Widiyandari, H.; Ogi, T.; Haerudin, H. NCA cathode material: Synthesis methods and performance enhancement efforts. *Mater. Res. Express* **2018**, *5*, 122001. [[CrossRef](#)]
20. Lee, K.-K.; Kim, K.-B. Electrochemical and Structural Characterization of LiNi<sub>1-y</sub>Co<sub>y</sub>O<sub>2</sub> (0 ≤ y ≤ 0.2) Positive Electrodes during Initial Cycling. *J. Electrochem. Soc.* **2000**, *147*, 1709–1717. [[CrossRef](#)]
21. Cheng, C.-X.; Tan, L.-T.; Liu, H.-W.; Huang, X.-T. High Rate Performances of the Cathode Material LiNi<sub>1/3</sub>Co<sub>1/3</sub>Mn<sub>1/3</sub>O<sub>2</sub> Synthesized Using Low Temperature Hydroxide Precipitation. *Mater. Res. Bull.* **2011**, *46*, 2032–2035. [[CrossRef](#)]
22. Tang, Z.-F.; Wang, S.; Liao, J.-Y.; Wang, S.; He, X.-D.; Pan, B.-C.; He, H.-Y.; Chen, C.-H. Facilitating lithium-ion diffusion in layered cathode materials by introducing Li<sup>+</sup>/Ni<sup>2+</sup> antisite defects for high-rate Li-ion batteries. *Research* **2019**, *2019*, 162–171. [[CrossRef](#)] [[PubMed](#)]
23. Ruan, Z.-W.; Zhu, Y.-M.; Teng, X.-G. Effect of pre-thermal treatment on the lithium storage performance of LiNi<sub>0.8</sub>Co<sub>0.15</sub>Al<sub>0.05</sub>O<sub>2</sub>. *J. Mater. Sci.* **2016**, *51*, 1400–1408. [[CrossRef](#)]
24. Vu, D.-L.; Choi, J.-Y.; Kim, W.-B.; Lee, J.-W. Layered LiNi<sub>0.8</sub>Co<sub>0.1</sub>Mn<sub>0.1</sub>O<sub>2</sub> prepared through calcination in air with preoxidized precursor. *J. Electrochem. Soc.* **2017**, *164*, A2670–A2676. [[CrossRef](#)]
25. Luo, Y.-H.; Pan, Q.-L.; Wei, H.-X.; Huang, Y.-D.; Tang, L.-B.; Wang, Z.-Y.; He, Z.-J.; Yan, C.; Mao, J.; Dai, K.-H.; et al. Towards Ni-rich layered oxides cathodes with low Li/Ni intermixing by mild molten-salt ion exchange for lithium-ion batteries. *Nano Energy* **2022**, *102*, 107626. [[CrossRef](#)]
26. Xiao, P.; Li, W.-H.; Chen, S.; Li, G.; Dai, Z.-J.; Feng, M.-D.; Chen, X.; Yang, W.-S. Effects of Oxygen pressurization on Li<sup>+</sup>/Ni<sup>2+</sup> cation mixing and the oxygen vacancies of LiNi<sub>0.8</sub>Co<sub>0.15</sub>Al<sub>0.05</sub>O<sub>2</sub> cathode materials. *ACS Appl. Mater. Inter.* **2022**, *14*, 31851–31861. [[CrossRef](#)]
27. Miller, D.-J.; Proff, C.; Wen, J.-G.; Daniel, P.-A.; Javier, B. Observation of microstructural evolution in Li battery cathode oxide particles by in situ electron microscopy. *Adv. Energy Mater.* **2013**, *3*, 1098–1103. [[CrossRef](#)]
28. Watanabe, S.; Kinoshita, M.; Hosokawa, T.; Morigaki, K.; Nakura, K. Capacity fade of LiAl<sub>y</sub>Ni<sub>1-x-y</sub>Co<sub>x</sub>O<sub>2</sub> cathode for lithium-ion batteries during accelerated calendar and cycle life tests surface analysis of LiAl<sub>y</sub>Ni<sub>1-x-y</sub>Co<sub>x</sub>O<sub>2</sub> cathode after cycle tests in restricted depth of discharge ranges. *J. Power Source* **2014**, *258*, 210–217. [[CrossRef](#)]
29. Eunmi, J.; Sooyeon, H.; Seung, M.-K.; Chang, W.-Y. Investigating the kinetic effect on structural evolution of Li<sub>x</sub>Ni<sub>0.8</sub>Co<sub>0.15</sub>Al<sub>0.05</sub>O<sub>2</sub> cathode materials during the initial charge/discharge. *Chem. Mater.* **2017**, *29*, 2708–2716.
30. Hwang, S.; Chang, W.; Kim, S.-M.; Su, D.; Dong, H.-K.; Lee, J.-Y.; Chung, K.-Y.; Eric, A.S. Investigation of changes in the surface-structure of LiNi<sub>0.8</sub>Co<sub>0.15</sub>Al<sub>0.05</sub>O<sub>2</sub> cathode materials induced by the initial charge. *Chem. Mater.* **2014**, *26*, 1084–1092. [[CrossRef](#)]
31. Yano, A.; Aoyama, S.; Shikano, M.; Shikano, M.; Sakaebe, H.; Tatsumi, K.; Ogumi, Z. Surface structure and high-voltage charge/discharge characteristics of Al-oxide coated LiNi<sub>1/3</sub>Co<sub>1/3</sub>Mn<sub>1/3</sub>O<sub>2</sub> cathodes. *J. Electrochem. Soc.* **2015**, *162*, A3137–A3144. [[CrossRef](#)]
32. Sallis, S.; Pereira, N.; Mukherjee, P.; Quackenbush, N.-F.; Faenza, N.; Schlueter, C.; Lee, T.-L.; Yang, W.-L.; Cosandey, F.; Amatucci, G.-G.; et al. Surface degradation of Li<sub>1-x</sub>Ni<sub>0.8</sub>Co<sub>0.15</sub>Al<sub>0.05</sub>O<sub>2</sub> cathodes: Correlating charge transfer impedance with surface phase transformations. *Appl. Phys. Lett.* **2016**, *108*, 263902. [[CrossRef](#)]
33. Chen, J.-N.; Yang, Y.; Tang, Y.-S.; Wang, Y.-F.; Li, H.; Xiao, X.-H.; Wang, S.-N.; Mariyam, S.D.D.; Etter, M.; Missyul, A.; et al. Constructing a thin disordered self-protective layer on the LiNiO<sub>2</sub> primary particles against oxygen release. *Adv. Funct. Mater.* **2022**, *33*, 2211515. [[CrossRef](#)]
34. Li, X.-H.; Wang, Q.; Guo, H.-Y.; Artrith, N.; Urban, A. Understanding the onset of surface degradation in LiNiO<sub>2</sub> cathodes. *ACS Appl. Energy Mater.* **2022**, *5*, 5730–5741. [[CrossRef](#)]
35. Wang, H.; Liu, F.; Yu, R.-N.; Xiao, Z.-T.; Zhu, Z.; Zhou, L.; Wu, J.-S. Co-gradient Li-rich cathode relieving the capacity decay in Lithium-ion batteries. *Nano Energy* **2022**, *100*, 107439. [[CrossRef](#)]

36. Zhang, D.-F.; Liu, M.; Ma, J.-B.; Yang, K.; Chen, Z.; Li, K.-K.; Zhang, C.; Wei, Y.-P.; Zhou, M.; Wang, P.; et al. Lithium hexamethyldisilazide as electrolyte additive for efficient cycling of high-voltage non-aqueous lithium metal batteries. *Nat. Commun.* **2022**, *13*, 6966. [CrossRef]
37. Lin, W.-C.; Ye, Y.-K.; Chen, T.-W.; Jiang, Y.; Ouyang, C.-Y.; Pan, F.; Zheng, J.-X. Defect-mediated Jahn-Teller effect in layered  $\text{LiNiO}_2$ . *Sci. China Mater.* **2022**, *65*, 1696–1700. [CrossRef]
38. Li, S.; Yao, Z.-P.; Zheng, J.-M.; Fu, M.-S.; Cen, J.-J.; Hwang, S.; Jin, H.; Orlov, A.; Gu, L.; Wang, S.; et al. Direct observation of defect-aided structural evolution in a nickel-rich layered cathode. *Angew. Chem. Int. Ed. Engl.* **2020**, *59*, 22092–22099. [CrossRef]
39. Zheng, J.-X.; Ye, Y.-K.; Liu, T.-C.; Xiao, Y.-G.; Wang, C.-M.; Wang, F.; Pan, F. Ni/Li disordering in layered transition metal oxide: Electrochemical impact, origin, and control. *Acc. Chem. Res.* **2019**, *52*, 2201–2209. [CrossRef]
40. Li, W.-D.; Asl, H.-Y.; Xie, Q.; Manthiram, A. Collapse of  $\text{LiNi}_{1-x-y}\text{Co}_x\text{Mn}_y\text{O}_2$  lattice at deep charge irrespective of nickel content in lithium-ion batteries. *J. Am. Chem. Soc.* **2019**, *141*, 5097–5101. [CrossRef]
41. Lee, J.; Urban, A.; Li, X.; Su, D.; Hautier, G.; Geder, G. Unlocking the potential of cation-disordered oxides for rechargeable lithium batteries. *Science* **2014**, *343*, 519–522. [CrossRef] [PubMed]
42. Ghosh, A.; Foster, J.-M.; Offer, G.; Marinescu, M. A shrinking-core model for the degradation of high-nickel cathodes (NMC811) in Li-ion batteries: Passivation layer growth and oxygen evolution. *J. Electrochem. Soc.* **2021**, *168*, 020509. [CrossRef]
43. Mikheenkova, A.; Gustafsson, O.; Misiewicz, C.; Brant, W.-R.; Hahlin, M.; Lacey, M.J. Resolving high potential structural deterioration in Ni-rich layered cathode materials for lithium-ion batteries operando. *J. Energy Storage* **2023**, *57*, 106211. [CrossRef]
44. Vetter, J.; Nov, K.-P.; Wagner, M.-R.; Viet, C.; Möller, K.-C.; Besenhard, J.-O.; Winte, M.; Wohlfahrt-Mehrens, M.; Vogler, C.; Hammouche, A. Ageing mechanisms in Lithium-ion batteries. *J. Power Sources* **2005**, *147*, 269–281. [CrossRef]
45. Edström, K.; Gustafsson, T.; Thomas, J.-O. The cathode–electrolyte interface in the Li-ion battery. *Electrochim. Acta* **2004**, *50*, 397–403. [CrossRef]
46. Gauthier, M.; Carney, T.-J.; Grimaud, A.; Giordano, L.; Pour, N.; Chang, H.-H.; Fenning, D.-P.; Lux, S.-F.; Paschos, O.; Bauer, C.; et al. Electrode-electrolyte interface in Li-ion batteries: Current understanding and new insights. *J. Phys. Chem. Lett.* **2015**, *6*, 4653–4672. [CrossRef]
47. Zheng, S.-J.; Huang, R.; Makimura, Y.; Ukyo, Y.; Fisher, C.A.J.; Hirayama, T.; Ikuhara, Y. Microstructural changes in  $\text{LiNi}_{0.8}\text{Co}_{0.15}\text{Al}_{0.05}\text{O}_2$  positive electrode material during the first cycle. *J. Electrochem. Soc.* **2011**, *158*, A357–A362. [CrossRef]
48. Makimura, Y.; Zheng, S.-J.; Ikuhara, Y.; Ukyo, Y. Microstructural observation of  $\text{LiNi}_{0.8}\text{Co}_{0.15}\text{Al}_{0.05}\text{O}_2$  after charge and discharge by scanning transmission electron microscopy. *J. Electrochem. Soc.* **2012**, *159*, A1070–A1073. [CrossRef]
49. Fu, C.-C.; Li, G.-S.; Luo, D.; Li, Q.; Fan, J.-M.; Li, L.-P. Nickel-rich layered microspheres cathodes: Lithium/nickel disordering and electrochemical performance. *ACS Appl. Mater. Interfaces* **2014**, *6*, 15822–15831. [CrossRef]
50. Bak, S.-M.; Hu, E.; Zhou, Y.-N.; Yu, X.-Q.; Senanayake, S.-D.; Cho, S.-J.; Kim, K.-B.; Chung, K.-Y.; Yang, X.-Q.; Nam, K.-W. Structural changes and thermal stability of charged  $\text{LiNi}_x\text{Mn}_y\text{Co}_z\text{O}_2$  cathode materials studied by combined in situ time-resolved XRD and mass spectroscopy. *ACS Appl. Mater. Interfaces* **2014**, *6*, 22594–22601. [CrossRef]
51. Bak, S.-M.; Nam, K.-W.; Chang, W.-Y.; Yu, X.-Q.; Hu, E.-Y.; Hwang, S.; Stach, E.-A.; Kim, K.-B.; Chung, K.-Y.; Yang, X.-Q. Correlating structural changes and gas evolution during the thermal decomposition of charged  $\text{Li}_x\text{Ni}_{0.8}\text{Co}_{0.15}\text{Al}_{0.05}\text{O}_2$  cathode materials. *Chem. Mater.* **2013**, *25*, 337–351. [CrossRef]
52. Yoon, C.-S.; Ryu, H.-H.; Park, G.-T.; Kim, J.-H.; Kim, K.-H.; Sun, Y.-K. Extracting maximum capacity from Ni-rich  $\text{Li}[\text{Ni}_{0.95}\text{Co}_{0.025}\text{Mn}_{0.025}]\text{O}_2$  cathode for high-energy-density lithium-ion batteries. *J. Mater. Chem. A* **2018**, *6*, 4126–4132. [CrossRef]
53. Miller, D.-J.; Proff, C.; Wen, J.-G.; Abraham, D.-P.; Bareño, J. Direct observation of microstructural evolution in Li battery cathode oxide particles during electrochemical cycling by in situ electron microscopy. *Microsc. Microanal.* **2012**, *18*, 1108–1109. [CrossRef]
54. Watanabe, S.; Kinoshita, M.; Hosokawa, T.; Morigaki, K.; Nakura, K. Capacity fading of  $\text{LiAl}_y\text{Ni}_{1-x-y}\text{Co}_x\text{O}_2$  cathode for lithium-ion batteries during accelerated calendar and cycle life tests (effect of depth of discharge in charge—Discharge cycling on the suppression of the micro-crack generation of  $\text{LiAl}_y\text{Ni}_{1-x-y}\text{Co}_x\text{O}_2$  particle). *J. Power Sources* **2014**, *260*, 50–56.
55. Ishidzu, K.; Oka, Y.; Nakamura, T. Lattice volume change during charge/discharge reaction and cycle performance of  $\text{Li}[\text{Ni}_x\text{Co}_y\text{Mn}_z]\text{O}_2$ . *Solid State Ion.* **2016**, *288*, 176–179. [CrossRef]
56. Palacín, M.-R.; Guibert, A.-D. Why do batteries fail. *Science* **2016**, *351*, 1253292. [CrossRef]
57. Kondrakov, A.-O.; Schmidt, A.; Xu, J.; Gesswein, H.; Monig, R.; Hartmann, P.; Sommer, H.; Brezesinski, T.; Janek, J. Anisotropic lattice strain and mechanical degradation of high- and low-nickel NCM cathode materials for Li-ion batteries. *J. Phys. Chem. C* **2017**, *121*, 3286–3294. [CrossRef]
58. Mukai, K. Pseudo zero-strain insertion materials for Li-ion batteries: Cross-sectional observations of  $\text{LiNi}_{1/2}\text{Co}_{1/2}\text{O}_2$ ,  $\text{LiNi}_{1/3}\text{Co}_{1/3}\text{Mn}_{1/3}\text{O}_2$ , and  $\text{LiNi}_{0.8}\text{Co}_{0.15}\text{Al}_{0.05}\text{O}_2$ . *Ionics* **2018**, *24*, 2181–2186. [CrossRef]
59. Lim, J.-M.; Hwang, T.; Kim, D.; Park, M.-S.; Cho, K.; Cho, M. Intrinsic origins of crack generation in Ni-rich  $\text{LiNi}_{0.8}\text{Co}_{0.1}\text{Mn}_{0.1}\text{O}_2$  layered oxide cathode material. *Sci. Rep.* **2017**, *7*, 39669–39679. [CrossRef]
60. Ryu, H.-H.; Park, K.-J.; Yoon, C.-S.; Sun, Y.-K. Capacity Fading of Ni-Rich  $\text{Li}[\text{Ni}_x\text{Co}_y\text{Mn}_{1-x-y}]\text{O}_2$  ( $0.6 \leq x \leq 0.95$ ) Cathodes for high-energy-density lithium-ion batteries: Bulk or surface degradation. *Chem. Mater.* **2018**, *30*, 1155–1163. [CrossRef]
61. Kim, J.; Lee, H.; Cha, H.; Yoon, M.; Park, M.; Cho, J. Prospect and reality of Ni-rich cathode for commercialization. *Adv. Energy Mater.* **2018**, *8*, 1702028. [CrossRef]

62. Mukhopadhyay, A.; Sheldon, B.-W. Deformation and stress in electrode materials for Li-ion batteries. *Prog. Mater. Sci.* **2014**, *63*, 58–116. [[CrossRef](#)]
63. Hua, W.-B.; Zhang, J.-L.; Wang, S.-N.; Cheng, Y.; Li, H.; Tseng, J.; Wu, Z.-H.; Shen, C.-H.; Dolotko, O.; Liu, H.; et al. Long-range cationic disordering induces two distinct degradation pathways in co-free Ni-rich layered cathodes. *Angew. Chem. Int. Ed.* **2022**, *62*, e202214880. [[CrossRef](#)]
64. Mao, Y.-W.; Wang, X.-L.; Xia, S.-H.; Zhang, K.; Wei, C.-X.; Bak, S.; Shadik, Z.; Liu, X.-J.; Yang, Y.; Xu, R.; et al. High-voltage charging-induced strain, heterogeneity, and micro-cracks in secondary particles of a nickel-rich layered cathode material. *Adv. Funct. Mater.* **2019**, *29*, 1900247. [[CrossRef](#)]
65. Park, S.-H.; Lee, H.; Park, J.; Roh, Y.; Byun, S.; Lim, J.; Jung, S.; Kim, N.; Lee, K.-T.; Lee, Y.-M. A microcrack propagation-based life prediction model for lithium-ion batteries with Ni-rich cathode materials. *J. Energy Storage* **2023**, *58*, 106420. [[CrossRef](#)]
66. Quilty, C.-D.; West, P.-J.; Li, W.-Z.; Dunkin, M.-R.; Wheeler, G.-P.; Ehrlich, S.; Ma, L.; Jaye, C.; Fischer, D.-A.; Takeuchi, E.-S.; et al. Multimodal electrochemistry coupled microcalorimetric and X-ray probing of the capacity fade mechanisms of Nickel rich NMC—progress and outlook. *Phys. Chem. Chem. Phys.* **2022**, *24*, 11471. [[CrossRef](#)]
67. Wu, L.-M.; Xiao, X.-H.; Wen, Y.-H.; Zhang, J. Three-dimensional finite element study on stress generation in synchrotron X-ray tomography reconstructed nickel-manganese cobalt based half cell. *J. Power Sources* **2016**, *336*, 8–18. [[CrossRef](#)]
68. Nam, G.-W.; Park, N.-Y.; Park, K.-J.; Yang, J.; Liu, J.; Yoon, C.-S.; Sun, Y.-K. Capacity fading of Ni-rich NCA cathodes: Effect of microcracking extent. *ACS Energy Lett.* **2019**, *4*, 2995–3001. [[CrossRef](#)]
69. Park, N.-Y.; Park, G.-T.; Kim, S.-B.; Jung, W.; Park, B.-C.; Sun, Y.-K. Degradation mechanism of Ni-rich cathode materials: Focusing on particle interior. *ACS Energy Lett.* **2022**, *7*, 2362–2369. [[CrossRef](#)]
70. Yoon, W.-S.; Balasubramanian, M.; Yang, X.-Q.; Mcbreen, J.; Hanson, J. Time-resolved XRD study on the thermal decomposition of  $\text{Li}_{1-x}\text{Ni}_{0.8}\text{Co}_{0.15}\text{Al}_{0.05}\text{O}_2$  cathode materials for Li-ion batteries. *Electrochem. Solid. St.* **2005**, *8*, A83–A86. [[CrossRef](#)]
71. Yoon, W.-S.; Hanson, J.; Mcbreen, J.; Yang, X.-Q. A study on the newly observed intermediate structures during the thermal decomposition of nickel-based layered cathode materials using time-resolved XRD. *Electrochem. Commun.* **2006**, *8*, 859–862. [[CrossRef](#)]
72. Yoon, W.-S.; Chung, K.-Y.; Balasubramanian, M.; Hanson, J.; Mcbreen, J.; Yang, X.-Q. Time-resolved XRD study on the thermal decomposition of nickel-based layered cathode materials for Li-ion batteries. *J. Power Sources* **2006**, *163*, 219–222. [[CrossRef](#)]
73. Wu, L.; Nam, K.-W.; Wang, X.; Zhou, Y.; Zheng, J.-C.; Yang, X.-Q.; Zhu, Y. Structural origin of overcharge-induced thermal instability of Ni-containing layered-cathodes for high-energy-density lithium batteries. *Chem. Mater.* **2011**, *23*, 3953–3960. [[CrossRef](#)]
74. Nam, K.-W.; Bak, S.-M.; Hu, E.; Yu, X.-Q.; Zhou, Y.; Wang, X.-J.; Wu, L.-J.; Zhu, Y.; Chung, K.-Y.; Yang, X.-Q. Combining in situ synchrotron X-Ray diffraction and absorption techniques with transmission electron microscopy to study the origin of thermal instability in overcharged cathode materials for lithium-ion batteries. *Adv. Funct. Mater.* **2013**, *23*, 1047–1063. [[CrossRef](#)]
75. Ma, L.; Nie, M.-Y.; Xia, J.; Dahn, J.R. A systematic study on the reactivity of different grades of charged  $\text{Li}[\text{Ni}_x\text{Mn}_y\text{Co}_z]\text{O}_2$  with electrolyte at elevated temperatures using accelerating rate calorimetry. *J. Power Sources* **2016**, *327*, 145–150. [[CrossRef](#)]
76. Walker, W.-Q.; Darst, J.-J.; Finegan, D.-P.; Bayles, G.-A.; Johnson, K.L.; Darcy, E.-C.; Rickman, S.-L. Decoupling of heat generated from ejected and non-ejected contents of 18650-format lithium-ion cells using statistical methods. *J. Power Sources* **2019**, *415*, 207–218. [[CrossRef](#)]
77. Noh, H.-J.; Yoon, S.-J.; Yoon, C.-S.; Sun, Y.-K. Comparison of the structural and electrochemical properties of layered  $\text{Li}[\text{Ni}_x\text{Co}_y\text{Mn}_z]\text{O}_2$  ( $x = 1/3, 0.5, 0.6, 0.7, 0.8, 0.85$ ) cathode material for lithium-ion batteries. *J. Power Sources* **2013**, *233*, 121–130. [[CrossRef](#)]
78. Gong, J.-Q.; Wang, Q.-S.; Sun, J.-H. Thermal analysis of nickel cobalt lithium manganese with varying nickel content used for lithium-ion batteries. *Thermochim. Acta* **2017**, *655*, 176–180. [[CrossRef](#)]
79. Shi, C.-G.; Peng, X.-X.; Dai, P.; Xiao, P.H.; Zheng, W.-C.; Li, H.-Y.; Li, H.; Indris, S.; Mangold, S.; Hong, Y.-H.; et al. Investigation and suppression of oxygen release by  $\text{LiNi}_{0.8}\text{Co}_{0.1}\text{Mn}_{0.1}\text{O}_2$  cathode under overcharge conditions. *Adv. Energy Mater.* **2022**, *12*, 2200569. [[CrossRef](#)]
80. Hayashi, T.; Okada, J.; Toda, E.; Kuzuo, R.; Oshimura, N.; Kuwata, N.; Kawamura, J. Degradation mechanism of  $\text{LiNi}_{0.82}\text{Co}_{0.15}\text{Al}_{0.03}\text{O}_2$  positive electrodes of a lithium-ion battery by a long-term cycling test. *J. Electrochem. Soc.* **2014**, *161*, A1007–A1011. [[CrossRef](#)]
81. Sun, H.-H.; Choi, W.; Lee, J.-K.; Oh, I.-H.; Jung, H.-G. Control of electrochemical properties of nickel-rich layered cathode materials for lithium-ion batteries by variation of the manganese to cobalt ratio. *J. Power Sources* **2015**, *275*, 877–883. [[CrossRef](#)]
82. Kim, H.-R.; Woo, S.-G.; Kim, J.-H.; Cho, W.; Kim, Y.-J. Capacity fading behavior of Ni-Rich layered cathode materials in li-ion full cells. *J. Electroanal. Chem.* **2016**, *782*, 168–173. [[CrossRef](#)]
83. Liu, J.; Bao, Z.-N.; Cui, Y.; Dufek, E.-J.; Goodenough, J.-B.; Khalifah, P.; Li, Q.-Y.; Liaw, B.-Y.; Liu, P.; Manthiram, A.; et al. Pathways for practical high-energy long-cycling lithium metal batteries. *Nat. Energy* **2019**, *4*, 180–186. [[CrossRef](#)]
84. Kim, K.; Hwang, D.; Kim, S.; Park, S.-O.; Cha, Y.; Lee, Y.-S.; Cho, J.; Kwak, S.-K.; Choi, N.-S. Cyclic aminosilane-based additive ensuring stable electrode–electrolyte interfaces in Li-ion batteries. *Adv. Energy Mater.* **2020**, *10*, 2000012. [[CrossRef](#)]
85. Yang, Y.; Xu, S.-M.; Xie, M.; He, Y.-H.; Huang, G.-Y.; Yang, Y.-C. Growth mechanisms for spherical mixed hydroxide agglomerates prepared by co-precipitation method: A case of  $\text{Ni}_{1/3}\text{Co}_{1/3}\text{Mn}_{1/3}(\text{OH})_2$ . *J. Alloy. Compd.* **2015**, *619*, 846–853. [[CrossRef](#)]

86. Huang, Y.; Wang, Z.-X.; Li, X.-H.; Guo, H.-J.; Wang, J.-X. Synthesis of  $\text{Ni}_{0.8}\text{Co}_{0.1}\text{Mn}_{0.1}(\text{OH})_2$  precursor and electrochemical performance of  $\text{LiNi}_{0.8}\text{Co}_{0.1}\text{Mn}_{0.1}\text{O}_2$  cathode material for lithium batteries. *Trans. Nonferrous Met. Soc. China* **2015**, *25*, 2253–2259. [CrossRef]
87. Kim, Y.; Kim, D. Synthesis of high-density nickel cobalt aluminum hydroxide by continuous coprecipitation method. *ACS Appl. Mater. Interfaces* **2012**, *4*, 586–589. [CrossRef]
88. Lee, S.-H.; Kwon, K.-Y.; Choi, B.-K.; Yoo, H.-D. A kinetic descriptor to optimize Co-precipitation of Nickel-rich cathode precursors for Lithium-ion batteries. *J. Electroanal. Chem.* **2022**, *924*, 116828. [CrossRef]
89. Wang, X.; Zhang, X.-M.; Zhang, C.-M.; Zhang, L.; Wen, J.-W.; Wang, C.-X.; Huang, G.-Y. Synthesis of high-nickel and high-performance ternary cathode materials through spent lithium-ion batteries recycling system. *Sustain. Chem. Pharm.* **2023**, *31*, 100959. [CrossRef]
90. Yang, C.-K.; Qi, L.-Y.; Zuo, Z.-C.; Wang, R.-N.; Ye, M.; Lu, J.; Zhou, H.-H. Insights into the inner structure of high-nickel agglomerate as high-performance lithium-ion cathodes. *J. Power Sources* **2016**, *331*, 487–494. [CrossRef]
91. Duan, D.-G.; Wu, C.; Cao, Y.-B.; Huang, D.-H.; Du, K.; Peng, Z.D.; Hu, G.-R. Enhanced compacting density and cycling performance of Ni-riched electrode via building mono dispersed micron scaled morphology. *J. Alloy. Compd.* **2017**, *695*, 91–99. [CrossRef]
92. Park, G.-T.; Park, N.-Y.; Noh, T.-C.; Namkoong, B.; Ryu, H.-H.; Shin, J.-Y.; Beierling, T.; Yoon, C.-S.; Sun, Y.-K. High-performance Ni-rich  $\text{Li}[\text{Ni}_{0.9-x}\text{Co}_{0.1}\text{Al}_x]\text{O}_2$  cathodes via multi-stage microstructural tailoring from hydroxide precursor to the lithiated oxide. *Energy Environ. Sci.* **2021**, *14*, 5084–5095. [CrossRef]
93. Wu, Z.-W.; Zhou, Y.; Hai, C.-X.; Zeng, J.-B.; Ren, X.-F.; Sun, Y.-X.; Shen, Y.; Li, X.; Dong, S.-D.; Zhang, G.-T. Improving electrochemical performance of NCM811 cathodes for lithium-ion batteries via consistently arranging the hexagonal nanosheets with exposed {104} facets. *Ceram. Int.* **2022**, *48*, 17279–17288. [CrossRef]
94. Kim, U.-H.; Myung, S.-T.; Yoon, C.-S.; Sun, Y.-G. Extending the battery life using an Al-doped  $\text{Li}[\text{Ni}_{0.76}\text{Co}_{0.09}\text{Mn}_{0.15}]\text{O}_2$  cathode with concentration gradients for lithium ion batteries. *ACS Energy Lett.* **2017**, *2*, 1848–1854. [CrossRef]
95. Kim, U.-H.; Lee, S.-B.; Ryu, J.-H.; Yoon, C.-S.; Sun, Y.-G. Optimization of Ni-rich  $\text{Li}[\text{Ni}_{0.92-x}\text{Co}_{0.04}\text{Mn}_{0.04}\text{Al}_x]\text{O}_2$  cathodes for high energy density lithium-ion batteries. *J. Power Sources* **2023**, *564*, 232850. [CrossRef]
96. You, Y.; Celio, H.; Li, J.; Dolocan, A.; Manthiram, A. Modified high-nickel cathodes with stable surface chemistry against ambient air for lithium-ion batteries. *Angew. Chem. Int. Ed.* **2018**, *57*, 6480–6485. [CrossRef]
97. Kim, U.-H.; Kuo, L.-Y.; Kaghazchi, P.; Yoon, C.-S.; Sun, Y.-K. Quaternary layered Ni-rich NCMA cathode for lithium-ion batteries. *ACS Energy Lett.* **2019**, *4*, 576–582. [CrossRef]
98. Yu, H.-F.; Cao, Y.-Q.; Chen, L.; Hu, Y.-J.; Duan, X.-Z.; Dai, S.; Li, C.-Z.; Jiang, H. Surface enrichment and diffusion enabling gradient-doping and coating of Ni-rich cathode toward Li-ion batteries. *Nat. Commun.* **2021**, *12*, 4564. [CrossRef]
99. Li, W.-D.; Lee, S.; Manthiram, A. High-Nickel NMA: A cobalt-free alternative to NMC and NCA cathodes for lithium-ion batteries. *Adv. Mater.* **2020**, *32*, 2002718. [CrossRef]
100. Xi, R.-H.; Zhang, J.-N.; Lan, Z.-W.; Yuan, Y.-X.; Kang, J.-L.; Li, Y.-Y.; Wang, J.-T.; Zhang, C.-H.; Hou, X.-Y. High-nickel and cobalt-free layered  $\text{LiNi}_{0.90}\text{Mn}_{0.06}\text{Al}_{0.04}\text{O}_2$  cathode for lithium-ion batteries. *Ceram. Int.* **2022**, *48*, 36690–36696. [CrossRef]
101. Liu, Q.; Wu, Z.; Sun, J.-Y.; Xu, R.-M.; Li, X.-W.; Yu, X.; Liu, Y. Facile synthesis of crack-free single-crystalline Al-doped Co-free Ni-rich cathode material for lithium-ion batteries. *Electrochim. Acta* **2023**, *437*, 141473. [CrossRef]
102. Li, Y.; Chang, S.-H.; Zheng, J.-C.; Zhang, D.-W.; Yang, J.-C.; Chen, Y.-X.; Guo, J.; Zhu, J.; Xiong, Y.; Li, W. Dual-modification of  $\text{Gd}_2\text{O}_3$  on the high-voltage electrochemical properties of  $\text{LiNi}_{0.8}\text{Co}_{0.1}\text{Mn}_{0.1}\text{O}_2$  cathode materials via the solid-state method. *J. Solid State Electrochem.* **2020**, *24*, 863–872. [CrossRef]
103. Schipper, F.; Dixit, M.; Kovacheva, D.; Talianker, M.; Haik, O.; Grinblat, J.; Erickson, E.; Ghanty, C.; Major, D.; Markovsky, B.; et al. Stabilizing nickel-rich layered cathode materials by a high-charge cation doping strategy: Zirconium-doped  $\text{LiNi}_{0.6}\text{Co}_{0.2}\text{Mn}_{0.2}\text{O}_2$ . *J. Mater.* **2016**, *4*, 16073–16084. [CrossRef]
104. Schipper, F.; Bouzarglo, H.; Dixit, M.; Erickson, E.-M.; Weigel, T.; Talianker, M.; Grinblat, J.; Burstein, L.; Schmidt, M.; Lampert, J.; et al. From surface  $\text{ZrO}_2$  coating to bulk Zr doping by high temperature annealing of nickel-rich lithiated oxides and their enhanced electrochemical performance in lithium-ion batteries. *Adv. Energy Mater.* **2018**, *8*, 1701682. [CrossRef]
105. Schmich, R.; Wagner, R.; Höppl, G.; Placke, T.; Winter, M. Performance and cost of materials for lithium-based rechargeable automotive batteries. *Nat. Energy* **2018**, *3*, 267–278. [CrossRef]
106. Che, W.; Wan, X.-W.; Zhang, D.-Y.; Chang, C.-K. Stabilized performance of  $\text{LiNi}_{0.90}\text{Co}_{0.07}\text{Al}_{0.03}\text{O}_2$  cathodes via  $\text{Zr}^{4+}$  doping upon 4.5 V application due to the suppression of H2-H3 phase transitions. *ACS Sustain. Chem. Eng.* **2021**, *9*, 5536–5545. [CrossRef]
107. Ni, J.-X.; Tan, Y.-Y.; Xu, K.; Jiang, Y.-J.; Chang, W.-Y.; Lai, C.-Y.; Liu, H. Cobalt-free nickel-rich layered  $\text{LiNi}_{0.9}\text{Al}_{0.1-x}\text{Zr}_x\text{O}_2$  cathode for high energy density and stable lithium-ion batteries. *J. Taiwan Inst. Chem. Eng.* **2022**, *136*, 104421. [CrossRef]
108. Du, R.; Bi, Y.-J.; Yang, W.-C.; Peng, Z.; Liu, M.; Liu, Y.; Wu, B.-M.; Yang, B.-C.; Ding, F.; Wang, D.-Y. Improved cyclic stability of  $\text{LiNi}_{0.8}\text{Co}_{0.1}\text{Mn}_{0.1}\text{O}_2$  via Ti substitution with a cut-off potential of 4.5V. *Ceram. Int.* **2015**, *41*, 7133–7139. [CrossRef]
109. Jiang, Y.; Bi, Y.-J.; Liu, M.; Peng, Z.; Huai, L.-Y.; Dong, P.; Duan, J.-G.; Chen, Z.-L.; Li, X.; Wang, D.-Y. Improved stability of Ni-rich cathode by the substitutive cations with stronger bonds. *Electrochim. Acta* **2018**, *268*, 41–48. [CrossRef]
110. Zhang, Z.; Hong, B.; Yi, M.-Y.; Fan, X.-M.; Zhang, Z.; Huang, X.-B.; Lai, Y.-Q. In situ co-doping strategy for achieving long-term cycle stability of single-crystal Ni-rich cathodes at high voltage. *Chem. Eng. J.* **2022**, *445*, 136825. [CrossRef]

111. Yang, Z.-F.; Wang, Z.-H.; Zhu, Y.-H.; Jiang, H.; Li, C.-Z. Enhancing surface-to-bulk stability of layered Co-free Ni-rich cathodes for long-life Li-ion batteries. *Battery Energy* **2022**, *2*, 20220048. [[CrossRef](#)]
112. Kaneda, H.; Koshika, Y.; Mori, K. Improving the cycling performance and thermal stability of  $\text{LiNi}_{0.6}\text{Co}_{0.2}\text{Mn}_{0.2}\text{O}_2$  cathode materials by Nb-doping and surface modification. *Int. J. Electrochem. Sc.* **2017**, *12*, 4640–4653. [[CrossRef](#)]
113. Liu, S.-Y.; Chen, X.; Zhao, J.-Y.; Su, J.-M.; Zhang, C.-C.; Huang, T.; Wu, J.-H.; Yu, A.-S. Uncovering the role of Nb modification in improving the structure stability and electrochemical performance of  $\text{LiNi}_{0.6}\text{Co}_{0.2}\text{Mn}_{0.2}\text{O}_2$  cathode charged at higher voltage of 4.5 V. *J. Power Sources* **2018**, *374*, 149–157. [[CrossRef](#)]
114. Liu, L.-H.; Li, M.-C.; Chu, L.-H.; Jiang, B.; Lin, R.-X.; Zhu, X.-P.; Cao, G.-Z. Layered ternary metal oxides: Performance degradation mechanisms as cathodes, and design strategies for high performance batteries. *Prog. Mater. Sci.* **2020**, *111*, 100655. [[CrossRef](#)]
115. Kim, U.-H.; Lee, S.-B.; Park, N.-Y.; Kim, S.-J.; Yoon, C.-S.; Sun, Y.-K. High-energy-density Li-ion battery reaching full charge in 12 min. *ACS Energy Lett.* **2022**, *7*, 3880–3888. [[CrossRef](#)]
116. Wang, J.-L.; Yi, Z.-C.; Liu, C.-J.; He, M.-Y.; Miao, C.; Li, J.-Q.; Xu, G.-L.; Xiao, W. Revealing the effect of  $\text{Nb}^{5+}$  on the electrochemical performance of nickel-rich layered  $\text{LiNi}_{0.83}\text{Co}_{0.11}\text{Mn}_{0.06}\text{O}_2$  oxide cathode for lithium-ion batteries. *J. Colloid Interface Sci.* **2023**, *635*, 295–304. [[CrossRef](#)] [[PubMed](#)]
117. Weigel, T.; Schipper, F.; Erickson, E.-M.; Susai, F.-A.; Markovsky, B.; Aurbach, D. Structural and electrochemical aspects of  $\text{LiNi}_{0.8}\text{Co}_{0.1}\text{Mn}_{0.1}\text{O}_2$  cathode materials doped by various cations. *ACS Energy Lett.* **2019**, *4*, 508–516. [[CrossRef](#)]
118. Kim, U.-H.; Park, G.-T.; Son, B.-K.; Nam, G.-W.; Liu, J.; Kuo, L.-Y.; Kaghazchi, P.; Yoon, C.-S.; Sun, Y.-K. Heuristic solution for achieving long-term cycle stability for Ni-rich layered cathodes at full depth of discharge. *Nat. Energy* **2020**, *5*, 860–869. [[CrossRef](#)]
119. Sun, H.-H.; Kim, U.-H.; Park, J.-H.; Park, S.-W.; Seo, D.-H.; Heller, A.; Mullins, C.-B.; Yoon, C.-S.; Sun, Y.-K. Transition metal-doped Ni-rich layered cathode materials for durable Li-ion batteries. *Nat. Commun.* **2021**, *12*, 6552. [[CrossRef](#)]
120. Kimura, N.; Seki, E.; Konishi, H.; Hirano, T.; Takahashi, S.; Ueda, A.; Horiba, T. Cycle deterioration analysis of 0.6 Ah-class lithium-ion cells with cell chemistry of  $\text{LiNi}_{0.6}\text{Co}_{0.2}\text{Mn}_{0.2}\text{O}_2$ -based/graphite. *J. Power Sources* **2016**, *332*, 187–192. [[CrossRef](#)]
121. Xue, L.-L.; Li, Y.-J.; Xu, B.; Chen, Y.-X.; Cao, G.-L.; Li, J.-G.; Deng, S.-Y.; Chen, Y.-J.; Chen, J. Effect of Mo doping on the structure and electrochemical performances of  $\text{LiNi}_{0.6}\text{Co}_{0.2}\text{Mn}_{0.2}\text{O}_2$  cathode material at high cut-off voltage. *J. Alloy. Compd.* **2018**, *748*, 561–568. [[CrossRef](#)]
122. Sattar, T.; Lee, S.-H.; Jin, B.-S.; Kim, H.-S. Influence of Mo addition on the structural and electrochemical performance of Ni-rich cathode material for lithium-ion batteries. *Sci. Rep.* **2020**, *10*, 8562. [[CrossRef](#)]
123. Park, G.-T.; Namkoong, B.; Kim, S.-B.; Liu, J.; Yoon, C.-S.; Sun, Y.-K. Introducing high-valence elements into cobalt-free layered cathodes for practical lithium-ion batteries. *Nat. Energy* **2022**, *7*, 946–954. [[CrossRef](#)]
124. Ryu, H.-H.; Park, G.-T.; Yoon, C.-S.; Sun, Y.-K. Suppressing detrimental phase transitions via tungsten doping of  $\text{LiNiO}_2$  cathode for next generation lithium-ion batteries. *J. Mater. Chem. A* **2019**, *7*, 18580–18588. [[CrossRef](#)]
125. Ryu, H.-H.; Park, K.-J.; Yoon, D.-R.; Aishova, A.; Yoon, C.-S.; Sun, Y.-K.  $\text{Li}[\text{Ni}_{0.9}\text{Co}_{0.09}\text{W}_{0.01}]\text{O}_2$ : A new type of layered oxide cathode with high cycling stability. *Adv. Energy Mater.* **2019**, *9*, 1902698. [[CrossRef](#)]
126. Kim, U.-H.; Park, N.-Y.; Park, G.-T.; Kim, H.; Yoon, C.-S.; Sun, Y.-K. High-energy W-doped  $\text{Li}[\text{Ni}_{0.95}\text{Co}_{0.04}\text{Al}_{0.01}]\text{O}_2$  cathodes for next-generation electric vehicles. *Energy Stor. Mater.* **2020**, *33*, 399–407. [[CrossRef](#)]
127. Wang, J.-L.; Liu, C.-J.; Wang, Q.; Xu, G.-L.; Miao, C.; Xu, M.-B.; Wang, C.-J.; Xiao, W. Investigation of  $\text{W}^{6+}$ -doped in high-nickel  $\text{LiNi}_{0.83}\text{Co}_{0.11}\text{Mn}_{0.06}\text{O}_2$  cathode materials for high-performance lithium-ion batteries. *J. Colloid Interface Sci.* **2022**, *628*, 338–349. [[CrossRef](#)]
128. Xiang, J.-F.; Chang, C.-X.; Zhang, F.; Sun, J.-T. Effects of Mg doping on the electrochemical properties of  $\text{LiNi}_{0.8}\text{Co}_{0.2}\text{O}_2$  cathode material. *J. Alloy. Compd.* **2009**, *475*, 483–487. [[CrossRef](#)]
129. Huang, B.; Li, X.-H.; Wang, Z.-X.; Guo, H.-J.; Xiong, X.-H. Synthesis of Mg-doped  $\text{LiNi}_{0.8}\text{Co}_{0.15}\text{Al}_{0.05}\text{O}_2$  oxide and its electrochemical behavior in high-voltage lithium-ion batteries. *Ceram. Int.* **2014**, *40*, 13223–13230. [[CrossRef](#)]
130. Laskar, M.-R.; Jackson, D.-H.-K.; Xu, S.-Z.; Hamers, R.-J.; Morgan, D.; Kuech, T.-F. Atomic layer deposited MgO: A lower overpotential coating for  $\text{LiNi}_{0.5}\text{Mn}_{0.3}\text{Co}_{0.2}\text{O}_2$  cathode. *ACS Appl. Mater. Interfaces* **2017**, *9*, 11231–11239. [[CrossRef](#)]
131. Yang, G.-J.; Kim, Y. Electrochemical properties of Mg-added lithium nickel cobalt oxide induced by structural characteristics depending on the synthetic process. *Ceram. Int.* **2018**, *44*, 2198–2203. [[CrossRef](#)]
132. Li, M.; Wang, H.-Y.; Zhao, L.-M.; Zhou, Y.; Zhang, F.; He, D.-N. Improving the electrochemical performance of lithium-rich oxide layer material with Mg and La co-doping. *J. Alloy. Compd.* **2019**, *782*, 451–460. [[CrossRef](#)]
133. Weber, R.; Li, H.-Y.; Chen, W.-F.; Kim, C.-Y.; Plucknett, K.; Dahn, J.-R. In situ XRD studies during synthesis of single-crystal  $\text{LiNiO}_2$ ,  $\text{LiNi}_{0.975}\text{Mg}_{0.025}\text{O}_2$ , and  $\text{LiNi}_{0.95}\text{Al}_{0.05}\text{O}_2$  cathode materials. *J. Electrochem. Soc.* **2020**, *167*, 100501. [[CrossRef](#)]
134. Liu, A.; Zhang, N.; Stark, J.E.; Arab, P.; Li, H.; Dahn, J.R. Synthesis of co-free Ni-rich single crystal positive electrode materials for lithium-ion batteries: Part I. two-step lithiation method for Al or Mg-Doped  $\text{LiNiO}_2$ . *J. Electrochem. Soc.* **2021**, *168*, 040531. [[CrossRef](#)]
135. Liu, A.; Zhang, N.; Stark, J.-E.; Arab, P.; Li, H.-Y.; Dahn, J.-R. Synthesis of Co-Free Ni-Rich Single Crystal Positive Electrode Materials for Lithium Ion Batteries: Part II. One-Step Lithiation Method of Mg-Doped  $\text{LiNiO}_2$ . *J. Electrochem. Soc.* **2021**, *168*, 050506. [[CrossRef](#)]
136. Yu, H.-F.; Zhu, H.-W.; Yang, Z.-F.; Liu, M.-M.; Jiang, H.; Li, C.-Z. Bulk Mg-doping and surface polypyrrole-coating enable high-rate and long-life for Ni-rich layered cathodes. *Chem. Eng. J.* **2021**, *412*, 128625. [[CrossRef](#)]

137. Chen, M.-M.; Zhao, E.-Y.; Chen, D.-F.; Wu, M.-M.; Han, S.-B.; Huang, Q.-Z.; Yang, L.-M.; Xiao, X.-L.; Hu, Z.-B. Decreasing Li/Ni disorder and improving the electrochemical performances of Ni-Rich  $\text{LiNi}_{0.8}\text{Co}_{0.1}\text{Mn}_{0.1}\text{O}_2$  by Ca doping. *Inorg. Chem.* **2017**, *56*, 8355–8362. [[CrossRef](#)]
138. Wang, L.-C.; Chu, Y.-Q.; Nong, Y.-T.; Zheng, F.-H.; Li, Y.; Huang, Y.-Z.; Li, Y.-H.; Pan, Q.-C.; Wang, H.-Q.; Li, Q.-Y. Sr-Based Sub/Surface Integrated Layer and Bulk Doping to Enhance High-Voltage Cycling of a Ni-Rich Cathode Material. *ACS Sustain. Chem. Eng.* **2022**, *10*, 7883–7895. [[CrossRef](#)]
139. Cui, Z.-H.; Xie, Q.; Manthiram, A. Zinc-Doped High-Nickel, Low-Cobalt Layered Oxide Cathodes for High-Energy-Density Lithium-Ion Batteries. *ACS Appl. Mater. Interfaces* **2021**, *13*, 15324–15332. [[CrossRef](#)]
140. Kim, Y. Lithium nickel cobalt manganese oxide synthesized using alkali chloride flux: Morphology and performance as a cathode material for lithium-ion batteries. *ACS Appl. Mater. Interfaces* **2012**, *4*, 2329–2333. [[CrossRef](#)]
141. Huang, Z.-J.; Wang, Z.-X.; Jing, Q.; Guo, H.-J.; Li, X.-H.; Yang, Z.-H. Investigation on the effect of Na doping on structure and Li-ion kinetics of layered  $\text{LiNi}_{0.6}\text{Co}_{0.2}\text{Mn}_{0.2}\text{O}_2$  cathode material. *Electrochim. Acta.* **2016**, *192*, 120–126. [[CrossRef](#)]
142. Wang, Y.-Y.; Sun, Y.-Y.; Liu, S.; Li, G.-R.; Gao, X.-P. Na-doped  $\text{LiNi}_{0.8}\text{Co}_{0.15}\text{Al}_{0.05}\text{O}_2$  with excellent stability of both capacity and potential as cathode materials for Li-ion batteries. *ACS Appl. Energy Mater.* **2018**, *1*, 3881–3889. [[CrossRef](#)]
143. Chen, T.; Li, X.; Wang, H.; Yan, X.-X.; Wang, L.; Deng, B.-W.; Ge, W.-J.; Qu, M.-Z. The effect of gradient boracic polyanion-doping on structure, morphology, and cycling performance of Ni-rich  $\text{LiNi}_{0.8}\text{Co}_{0.15}\text{Al}_{0.05}\text{O}_2$  cathode material. *J. Power Sources* **2018**, *374*, 1–11. [[CrossRef](#)]
144. Park, K.-J.; Jung, H.-G.; Kuo, L.-Y.; Kaghazchi, P.; Yoon, C.-S.; Sun, Y.-K. Improved cycling stability of  $\text{Li}[\text{Ni}_{0.90}\text{Co}_{0.05}\text{Mn}_{0.05}]\text{O}_2$  through microstructure modification by boron doping for Li-ion batteries. *Adv. Energy Mater.* **2018**, *8*, 1801202. [[CrossRef](#)]
145. Ryu, H.-H.; Park, N.-Y.; Seo, J.-H.; Yu, Y.-S.; Sharma, M.; Mucke, R.; Kaghazchi, P.; Yoon, C.-S.; Sun, Y.-K. A highly stabilized Ni-rich NCA cathode for high-energy lithium-ion batteries. *Mater. Today* **2020**, *36*, 73–82. [[CrossRef](#)]
146. Liu, Y.; Fan, X.-M.; Luo, B.; Zhao, Z.-W.; Shen, J.-X.; Liu, Z.-H.; Xiao, Z.-M.; Zhang, B.; Zhang, J.-F.; Ming, L. Understanding the enhancement effect of boron doping on the electrochemical performance of single-crystalline Ni-rich cathode materials. *J. Colloid Interface Sci.* **2021**, *604*, 776–784. [[CrossRef](#)]
147. Yue, P.; Wang, Z.-X.; Guo, H.-J.; Xiong, X.-H.; Li, X.-H. A low temperature fluorine substitution on the electrochemical performance of layered  $\text{LiNi}_{0.8}\text{Co}_{0.1}\text{Mn}_{0.1}\text{O}_{2-z}\text{F}_z$  cathode materials. *Electrochim. Acta* **2013**, *92*, 1–8. [[CrossRef](#)]
148. Li, X.; Xie, Z.-W.; Liu, W.-J.; Ge, W.-J.; Wang, H.; Qu, M.-Z. Effects of fluorine doping on structure, surface chemistry, and electrochemical performance of  $\text{LiNi}_{0.8}\text{Co}_{0.15}\text{Al}_{0.05}\text{O}_2$ . *Electrochim. Acta* **2015**, *174*, 1122–1130. [[CrossRef](#)]
149. Kong, F.-T.; Liang, C.-P.; Longo, R.-C.; Yeon, D.-H.; Zheng, Y.-P.; Park, J.-H.; Doo, S.-G.; Cho, K. Conflicting roles of anion doping on the electrochemical performance of Li-ion battery cathode materials. *Chem. Mater.* **2016**, *28*, 6942–6952. [[CrossRef](#)]
150. Binder, J.-O.; Culver, S.-P.; Pinedo, R.; Weber, D.-A.; Friedrich, M.-S.; Gries, K.-I.; Volz, K.; Zeier, W.-G.; Janek, J. Investigation of fluorine and nitrogen as anionic dopants in nickel-rich cathode materials for lithium-ion batteries. *ACS Appl. Mater. Interfaces* **2018**, *10*, 44452–44462. [[CrossRef](#)]
151. Li, C.-L.; Kan, W.-H.; Xie, H.-L.; Jiang, Y.; Zhao, Z.-K.; Zhu, C.-Y.; Xia, Y.-H.; Zhang, J.; Xu, K.; Mu, D.-B.; et al. Inducing favorable cation antisite by doping halogen in Ni-rich layered cathode with ultrahigh stability. *Adv. Sci.* **2018**, *6*, 1801406. [[CrossRef](#)] [[PubMed](#)]
152. Xie, J.; Sendek, A.-D.; Cubuk, E.-D.; Zhang, X.-K.; Lu, Z.-Y.; Gong, Y.-J.; Wu, T.; Shi, F.-F.; Liu, W.; Reed, E.-J. Atomic layer deposition of stable  $\text{LiAlF}_4$  lithium-ion conductive interfacial layer for stable cathode cycling. *ACS Nano* **2017**, *11*, 7019–7027. [[CrossRef](#)] [[PubMed](#)]
153. Vanaphuti, P.; Chen, J.-J.; Cao, J.-Y.; Bigham, K.; Chen, B.; Yang, L.-F.; Chen, H.-L.; Wang, Y. Enhanced electrochemical performance of the lithium-manganese-rich cathode for Li-ion batteries with Na and F codoping. *ACS Appl. Mater. Interfaces* **2019**, *11*, 37842–37849. [[CrossRef](#)] [[PubMed](#)]
154. Seo, J.-H.; Kim, U.-H.; Sun, Y.-K.; Yoon, C.-S. Multi-Doped (Ga,B)  $\text{Li}[\text{Ni}_{0.885}\text{Co}_{0.100}\text{Al}_{0.015}]\text{O}_2$  Cathode. *J. Electrochem. Soc.* **2020**, *167*, 100557. [[CrossRef](#)]
155. Feng, Z.; Rajagopalan, R.; Zhang, S.; Sun, D.; Tang, Y.-G.; Ren, Y.; Wang, H.-Y. A three in one strategy to achieve zirconium doping, boron doping, and interfacial coating for stable  $\text{LiNi}_{0.8}\text{Co}_{0.1}\text{Mn}_{0.1}\text{O}_2$  cathode. *Adv. Sci.* **2020**, *8*, 2001809. [[CrossRef](#)]
156. Choi, C.-M.; Park, J.-H.; Sun, Y.-K.; Yoon, C.-S. Ultra-stable cycling of multi-doped (Zr,B)  $\text{Li}[\text{Ni}_{0.885}\text{Co}_{0.100}\text{Al}_{0.015}]\text{O}_2$  cathode. *J. Power Sources* **2021**, *513*, 230548. [[CrossRef](#)]
157. Darjazi, H.; Gonzalo, E.; Acebedo, B.; Cid, R.; Zarrabeitia, M.; Bonilla, F. Improving high-voltage cycling performance of Nickel-rich NMC layered oxide cathodes for rechargeable lithium-ion batteries by Mg and Zr co-doping. *Mater. Today* **2022**, *20*, 100236.
158. Ryu, H.-H.; Lim, H.-W.; Kang, G.-C.; Park, N.-Y.; Sun, Y.-K. Long-Lasting Ni-Rich NCMA Cathodes via Simultaneous Microstructural Refinement and surface Modification. *ACS Energy Lett.* **2023**, *8*, 1354–1361. [[CrossRef](#)]
159. Omanda, H.; Brousse, T.; Marhic, C.; Schleich, D.-M. Improvement of the thermal stability of  $\text{LiNi}_{0.8}\text{Co}_{0.2}\text{O}_2$  cathode by a  $\text{SiO}_x$  protective coating. *J. Electrochem. Soc.* **2004**, *151*, A922–A929. [[CrossRef](#)]
160. Cho, W.; Kim, S.-M.; Song, J.-H.; Yim, T.; Kim, J.-S.; Kim, Y.-J. Improved electrochemical and thermal properties of nickel rich  $\text{LiNi}_{0.6}\text{Co}_{0.2}\text{Mn}_{0.2}\text{O}_2$  cathode materials by  $\text{SiO}_2$  coating. *J. Power Sources* **2015**, *282*, 45–50. [[CrossRef](#)]

161. Han, B.; Xu, S.; Zhao, S.; Lin, G.-X.; Feng, Y.-Z.; Chen, L.-B.; Ivey, G.-D.; Wang, P.; Wei, W.-F. Enhancing the structural stability of Ni-rich layered oxide cathodes with a preformed Zr-concentrated defective nanolayer. *ACS Appl. Mater. Interfaces* **2018**, *10*, 39599–39607. [CrossRef]
162. Xu, Y.; Li, X.-H.; Wang, Z.-X.; Guo, H.-J.; Huang, B. Structure and electrochemical performance of TiO<sub>2</sub>-coated LiNi<sub>0.80</sub>Co<sub>0.15</sub>Al<sub>0.05</sub>O<sub>2</sub> cathode material. *Mater. Lett.* **2015**, *143*, 151–154. [CrossRef]
163. Li, W.-W.; Zhang, X.-J.; Si, J.-J.; Yang, J.; Sun, X.-Y. TiO<sub>2</sub>-coated LiNi<sub>0.9</sub>Co<sub>0.08</sub>Al<sub>0.02</sub>O<sub>2</sub> cathode materials with enhanced cycle performance for Li-ion batteries. *Rare Met.* **2021**, *40*, 1719–1726. [CrossRef]
164. Wang, W.-C.; Lee, C.-H.; Yu, D.; Kondo, Y.; Miyahara, Y.; Abe, T.; Miyazaki, K. Effects of a solid solution outer layer of TiO<sub>2</sub> on the surface and electrochemical properties of LiNi<sub>0.6</sub>Co<sub>0.2</sub>Mn<sub>0.2</sub>O<sub>2</sub> cathodes for lithium-ion batteries through the use of thin-film electrodes. *ACS Appl. Energy Mater.* **2022**, *5*, 5117–5126. [CrossRef]
165. Neudeck, S.; Strauss, F.; Garcia, G.; Wolf, H.; Janek, J.; Hartmann, P.; Brezesinski, T. Room temperature, liquid-phase Al<sub>2</sub>O<sub>3</sub> surface coating approach for Ni-rich layered oxide cathode material. *Chem. Commun.* **2019**, *55*, 2174–2177. [CrossRef]
166. Mohanty, D.; Dahlberg, K.; King, D.-M.; David, L.-A.; Sefat, A.-S.; Wood, D.-L.; Daniel, C.; Dhar, S.; Mahajan, V.; Lee, M.; et al. Modification of Ni-rich FCG NMC and NCA cathodes by atomic layer deposition: Preventing surface phase transitions for high-voltage lithium-ion batteries. *Sci. Rep.* **2016**, *6*, 26532. [CrossRef]
167. Lou, F.-H.; Xie, Q.-S.; Luo, X.-J.; Xie, Y.-T.; Wang, M.-Y.; Hao, H.-M.; Wang, Z.-Q.; Yang, L.-X.; Wang, G.; Chen, J.-Y.; et al. Preventing structural collapse and thermal runaway to improve the electrochemical performance and safety of LiNi<sub>0.8</sub>Co<sub>0.1</sub>Mn<sub>0.1</sub>O<sub>2</sub> by a negative-thermal-expansion material of Al<sub>2</sub>(WO<sub>3</sub>)<sub>4</sub>. *Ind. Eng. Chem. Res.* **2022**, *61*, 4588–4600. [CrossRef]
168. Zhang, X.-Y.; Qiu, Y.-G.; Cheng, F.-Y.; Wei, P.; Li, Y.-Y.; Liu, Y.; Sun, S.-X.; Xu, Y.; Li, Q.; Fang, C.; et al. Realization of a high-voltage and high-rate nickel-rich NCM cathode material for LIBs by Co and Ti dual modification. *ACS Appl. Mater. Interfaces* **2021**, *13*, 17707–17716. [CrossRef]
169. Yoon, M.; Dong, Y.-H.; Hwang, J.; Sung, J.; Cha, H.; Ahn, K.; Huang, Y.; Kang, S.-J.; Cho, J. Reactive boride infusion stabilizes Ni-rich cathodes for lithium-ion batteries. *Nat. Energy* **2021**, *6*, 362–371. [CrossRef]
170. Xiao, P.; Cao, Y.; Li, W.-H.; Li, G.; Yu, Y.-L.; Dai, Z.-J.; Du, Z.-X.; Chen, X.; Sun, J.; Yang, W.-S. simple strategy for synthesizing LiNi<sub>0.8</sub>Co<sub>0.15</sub>Al<sub>0.05</sub>O<sub>2</sub> using Co Al-LDH nanosheet-coated Ni(OH)<sub>2</sub> as the precursor: Dual effects of the buffer layer and synergistic diffusion. *ACS Appl. Mater. Interfaces* **2021**, *13*, 29714–29725. [CrossRef]
171. Zhang, X.-Y.; Zhang, P.-P.; Zeng, T.-Y.; Yu, Z.-L.; Qu, X.-Y.; Peng, X.-Q.; Zhou, Y.; Duan, X.-G.; Dou, A.; Su, M.; et al. Improving the structure stability of LiNi<sub>0.8</sub>Co<sub>0.15</sub>Al<sub>0.05</sub>O<sub>2</sub> by double modification of tantalum surface coating and doping. *ACS Appl. Energy Mater.* **2021**, *4*, 8641–8652. [CrossRef]
172. Cai, M.-Z.; Dong, Y.-H.; Xie, M.; Dong, W.-J.; Dong, C.-L.; Dai, P.; Zhang, H.; Wang, X.; Sun, X.-Z.; Zhang, S.-N.; et al. Stalling oxygen evolution in high-voltage cathodes by lanthanization. *Nat. Energy* **2023**, *8*, 159–168. [CrossRef]
173. Kim, H.-B.; Park, B.-C.; Myung, S.-T.; Amine, K.; Prakash, J.; Sun, Y.-K. Electrochemical and thermal characterization of AlF<sub>3</sub>-coated LiNi<sub>0.8</sub>Co<sub>0.15</sub>Al<sub>0.05</sub>O<sub>2</sub> cathode in lithium-ion cells. *J. Power Sources* **2008**, *179*, 347–350. [CrossRef]
174. Park, B.-C.; Kim, H.-B.; Bang, H.-J.; Prakash, J. Improvement of electrochemical performance of Li[Ni<sub>0.8</sub>Co<sub>0.15</sub>Al<sub>0.05</sub>]O<sub>2</sub> cathode materials by AlF<sub>3</sub> coating at various temperatures. *Ind. Eng. Chem. Res.* **2008**, *47*, 3876–3882. [CrossRef]
175. Xiong, X.-H.; Wang, Z.-X.; Yin, X.; Guo, H.-J.; Li, X.-H. A modified LiF coating process to enhance the electrochemical performance characteristics of LiNi<sub>0.8</sub>Co<sub>0.1</sub>Mn<sub>0.1</sub>O<sub>2</sub> cathode materials. *Mater. Lett.* **2013**, *110*, 4–9. [CrossRef]
176. Kim, Y.; Cho, J. Lithium-reactive Co<sub>3</sub>(PO<sub>4</sub>)<sub>2</sub> nanoparticle coating on high-capacity LiNi<sub>0.8</sub>Co<sub>0.16</sub>Al<sub>0.04</sub>O<sub>2</sub> cathode material for lithium rechargeable batteries. *J. Electrochem. Soc.* **2007**, *154*, A495–A499. [CrossRef]
177. Lee, D.-J.; Scrosati, B.; Sun, Y.-K. Ni<sub>3</sub>(PO<sub>4</sub>)<sub>2</sub>-coated Li[Ni<sub>0.8</sub>Co<sub>0.15</sub>Al<sub>0.05</sub>]O<sub>2</sub> lithium battery electrode with improved cycling performance at 55 °C. *J. Power Sources* **2011**, *196*, 7742–7746. [CrossRef]
178. Jo, M.; Oh, P.; Kim, J.; Choi, J.-H.; Kim, S.; Ha, S.; Son, Y. Electrochemical lithium storage performance at high voltage and temperature of LiNi<sub>0.6</sub>Co<sub>0.2</sub>Mn<sub>0.2</sub>O<sub>2</sub> cathode for Lithium-ion batteries by facile Mn<sub>3</sub>(PO<sub>4</sub>)<sub>2</sub> dry coating. *Appl. Surf. Sci.* **2013**, *613*, 156018. [CrossRef]
179. Huang, B.; Li, X.-H.; Wang, Z.-X.; Guo, H.-J. A facile process for coating amorphous FePO<sub>4</sub> onto LiNi<sub>0.8</sub>Co<sub>0.15</sub>Al<sub>0.05</sub>O<sub>2</sub> and the effects on its electrochemical properties. *Mater. Lett.* **2014**, *131*, 210–213. [CrossRef]
180. Qi, R.; Shi, J.-L.; Zhang, X.-D.; Zeng, X.-X. Improving the stability of LiNi<sub>0.80</sub>Co<sub>0.15</sub>Al<sub>0.05</sub>O<sub>2</sub> by AlPO<sub>4</sub> nanocoating for lithium-ion batteries. *Sci. China Chem.* **2017**, *60*, 1230–1235. [CrossRef]
181. Cheng, W.-D.; Li, L.; Hao, S.-L.; Wu, Y.-X.; Huo, J.-S.; Ji, Y.-Y.; Liu, X.-Q. Face-lifting the surface of LiNi<sub>0.8</sub>Co<sub>0.15</sub>Al<sub>0.05</sub>O<sub>2</sub> cathode via Y(PO<sub>3</sub>)<sub>3</sub> to form an in situ triple composite Li-ion conductor coating layer with the enhanced electrochemical performance. *Nanotechnology* **2022**, *33*, 375701. [CrossRef]
182. Peng, Z.-D.; Huang, M.; Wang, W.-G.; Du, K.; Guan, D.-C.; Hu, G.; Cao, Y.-B. Enhancing the structure and interface stability of LiNi<sub>0.83</sub>Co<sub>0.12</sub>Mn<sub>0.05</sub>O<sub>2</sub> cathode material for Li-ion batteries via facile CeP<sub>2</sub>O<sub>7</sub> coating. *ACS Sustain. Chem. Eng.* **2022**, *10*, 4881–4893. [CrossRef]
183. Wu, Y.-X.; Cheng, W.-D.; Hao, S.; Li, L.; Ran, Q.-W.; Liu, L.; Ji, Y.-Y.; Huo, J.-S.; Liu, X.-Q. Utilizing dual functions of LaPO<sub>4</sub> to enhance the electrochemical performance of LiNi<sub>0.87</sub>Co<sub>0.09</sub>Al<sub>0.04</sub>O<sub>2</sub> cathode material. *Nanotechnology* **2023**, *34*, 075706. [CrossRef]
184. Liu, W.-M.; Hu, G.-R.; Du, K.; Peng, Z.-D.; Cao, Y.-B. Surface coating of LiNi<sub>0.8</sub>Co<sub>0.15</sub>Al<sub>0.05</sub>O<sub>2</sub> with LiCoO<sub>2</sub> by a molten salt method. *Surf. Coat. Technol.* **2013**, *216*, 267–272. [CrossRef]

185. Yang, C.-K.; Shao, R.; Mi, Y.-Y.; Shen, L.-Y.; Zhao, B.-L.; Wang, Q.; Wu, K.; Lui, W.; Gao, P.; Zhou, H.-H. Stable interstitial layer to alleviate fatigue fracture of high nickel cathode for lithium-ion batteries. *J. Power Sources* **2018**, *376*, 200–206. [[CrossRef](#)]
186. Ito, S.; Fujiki, S.; Yamada, T.; Aihara, Y.; Park, Y.; Kim, T.-Y.; Baek, S.-W.; Lee, J.-M.; Doo, S.; Machida, N. A rocking chair type all-solid-state lithium-ion battery adopting  $\text{Li}_2\text{O-ZrO}_2$  coated  $\text{LiNi}_{0.8}\text{Co}_{0.15}\text{Al}_{0.05}\text{O}_2$  and a sulfide based electrolyte. *J. Power Sources* **2014**, *248*, 943–950. [[CrossRef](#)]
187. Song, B.-H.; Li, W.-D.; Oh, S.-M.; Manthiram, A. Long-life nickel-rich layered oxide cathodes with a uniform  $\text{Li}_2\text{ZrO}_3$  surface coating for lithium-ion batteries. *ACS Appl. Mater. Interfaces* **2017**, *9*, 9718–9725. [[CrossRef](#)]
188. Sun, X.-W.; Wang, L.-L.; Ma, J.; Yu, X.-R.; Zhang, S.; Zhou, X.-H.; Cui, G.-L. A Bifunctional Chemomechanics Strategy to Suppress Electrochemo-Mechanical Failure of Ni-Rich Cathodes for All-Solid-State Lithium Batteries. *ACS Appl. Mater. Interfaces* **2022**, *14*, 17674–17681. [[CrossRef](#)]
189. Jeyakumar, J.; Wu, Y.-S.; Wu, S.-H.; Jose, R.; Yang, C.-C. Surface-modified quaternary layered Ni-rich cathode materials by  $\text{Li}_2\text{ZrO}_3$  for improved electrochemical performance for high-power Li-ion batteries. *ACS Appl. Energy Mater.* **2022**, *5*, 4796–4807. [[CrossRef](#)]
190. Song, Y.; Hu, Y.; Guo, F.-Q.; Zhu, C.-Q.; Qiu, L.; Zhou, J.-B.; Deng, Y.-T.; Zheng, Z.; Liu, Y.; Sun, Y.; et al. Effective and low-cost in situ surface engineering strategy to enhance the interface stability of an ultrahigh Ni-rich NCMA cathode. *ACS Appl. Mater. Interfaces* **2022**, *14*, 51835–51845.
191. Qiao, Y.; Hao, R.-H.; Shi, X.-W.; Li, Y.-B.; Wang, Y.-L.; Zhang, Y.; Tang, C.; Li, G.-H.; Wang, G.-L.; Liu, J.-M.; et al. Improving the cycling stability of  $\text{LiNi}_{0.8}\text{Co}_{0.1}\text{Mn}_{0.1}\text{O}_2$  by enhancing the structural integrity via synchronous  $\text{Li}_2\text{SiO}_3$  coating. *ACS Appl. Energy Mater.* **2022**, *5*, 4885–4892. [[CrossRef](#)]
192. Huang, X.; Zhu, W.; Yao, J.; Bu, L.; Li, X.; Tian, K.; Lu, H.; Quan, C.; Xu, S.; Xu, K.; et al. Suppressing structural degradation of Ni-rich cathode materials towards improved cycling stability enabled by a  $\text{Li}_2\text{MnO}_3$  coating. *J. Mater. Chem. A* **2020**, *8*, 17429–17441. [[CrossRef](#)]
193. Kim, A.-Y.; Strauss, F.; Bartsch, T.; Teo, J.-H.; Janek, J.; Brezesinski, T. Effect of surface carbonates on the cyclability of  $\text{LiNbO}_3$ -coated NCM622 in all-solid-state batteries with lithium thiophosphate electrolytes. *Sci. Rep.* **2021**, *11*, 5367. [[CrossRef](#)] [[PubMed](#)]
194. Liu, H.-X.; Zhao, X.-Y.; Xie, Y.-G.; Luo, S.; Wang, Z.Y.; Zhu, L.-Y.; Zhang, X. Insights into capacity fading mechanism and coating modification of high-nickel cathodes in lithium-ion batteries. *ACS Appl. Mater. Interfaces* **2022**, *14*, 55491–55502. [[CrossRef](#)]
195. Chen, J.-H.; Zhu, L.; Jia, D.; Jiang, X.-B.; Wu, Y.-G.; Hao, O.-L.; Xia, X.-F.; Ouyang, Y.; Peng, L.; Tang, W.-P.; et al.  $\text{LiNi}_{0.8}\text{Co}_{0.15}\text{Al}_{0.05}\text{O}_2$  cathodes exhibiting improved capacity retention and thermal stability due to a lithium iron phosphate coating. *Electrochim* **2019**, *312*, 179–187. [[CrossRef](#)]
196. Zhang, J.-R.; Lan, Z.W.; Xi, R.-H.; Li, Y.-Y.; Zhang, C.-H. The cycle stability and rate performance of  $\text{LiNi}_{0.8}\text{Mn}_{0.1}\text{Co}_{0.1}\text{O}_2$  enhanced by Mg doping and  $\text{LiFePO}_4$  coating. *ChemElectroChem* **2022**, *9*, e202101654.
197. Tang, Z.-F.; Wu, R.; Huang, P.-F.; Wang, Q.-S.; Chen, C.-H. Improving the electrochemical performance of Ni-rich cathode material  $\text{LiNi}_{0.815}\text{Co}_{0.15}\text{Al}_{0.035}\text{O}_2$  by removing the lithium residues and forming  $\text{Li}_3\text{PO}_4$  coating layer. *J. Alloy. Compd.* **2017**, *693*, 1157–1163. [[CrossRef](#)]
198. Yan, P.-F.; Zheng, J.-M.; Liu, J.; Wang, B.-Q.; Cheng, X.-P.; Zhang, Y.-F.; Sun, C.-M.; Wang, X.-L.; Zhang, J.-G. Tailoring grain boundary structures and chemistry of Ni-rich layered cathodes for enhanced cycle stability of lithium-ion batteries. *Nat. Energy* **2018**, *3*, 600–605. [[CrossRef](#)]
199. Sattar, T.; Sim, S.-J.; Jin, B.-S.; Kim, H.-S. Dual function Li-reactive coating from residual lithium-on Ni-rich NCM cathode material for Lithium-ion batteries. *Sci. Rep.* **2021**, *11*, 18590. [[CrossRef](#)]
200. Cheng, W.-D.; Hao, S.; Ji, Y.-Y.; Li, L.; Liu, L.; Xiao, Y.; Wu, Y.-X.; Huo, J.-S.; Tang, F.; Liu, X.-Q. Optimizing surface residual alkali and enhancing electrochemical performance of  $\text{LiNi}_{0.8}\text{Co}_{0.15}\text{Al}_{0.05}\text{O}_2$  cathode by  $\text{LiH}_2\text{PO}_4$ . *Nanotechnology* **2022**, *33*, 045404. [[CrossRef](#)]
201. Du, F.-H.; Sun, P.-P.; Zhou, Q.; Zeng, D.; Hu, D.; Fan, Z.-X.; Hao, Q.; Mei, C.-X.; Xu, T.; Zheng, J.-W. Interlinking primary grains with lithium boron oxide to enhance the stability of  $\text{LiNi}_{0.8}\text{Co}_{0.15}\text{Al}_{0.05}\text{O}_2$ . *ACS Appl. Mater. Interfaces* **2020**, *12*, 56963–56973. [[CrossRef](#)]
202. Tan, X.-X.; Peng, W.-J.; Duan, H.; Wang, Z.-X.; Guo, H.-J.; Luo, G.; Yuan, R.-Z.; Li, X.-H.; Wang, J.-X. A scalable dry chemical method for lithium borate coating to improve the performance of  $\text{LiNi}_{0.90}\text{Co}_{0.06}\text{Mn}_{0.04}\text{O}_2$  cathode material. *Solid State Ion.* **2022**, *28*, 2073–2082. [[CrossRef](#)]
203. Yang, J.-C.; Li, Y.-J.; Xi, X.-M.; Zheng, J.-C.; Yu, J.; He, Z.-J. Suppressed internal intrinsic stress engineering in high-performance Ni-Rich cathode via multilayered in situ coating structure. *Energy Environ. Mater.* **2022**, *24*, 12574. [[CrossRef](#)]
204. Xia, Y.; Chen, A.-Q.; Wang, K.; Mao, Q.-Z.; Huang, H.; Zhang, J.; He, X.-P.; Gan, Y.-P.; Xiao, Z.; Zhang, W.-K. Industrial modification comparison of Ni-Rich cathode materials towards enhanced surface chemical stability against ambient air for advanced lithium-ion batteries. *Chem. Eng. J.* **2022**, *450*, 138382. [[CrossRef](#)]
205. Sattar, T.; Sim, S.-J.; Doo, S.-G.; Jin, B.-S.; Kim, H.-S. A synergetic modification approach toward high capacity Ni-rich cathode materials for next generation lithium-ion batteries. *Solid State Ion.* **2022**, *387*, 116053. [[CrossRef](#)]
206. Lv, Y.; Huang, S.-F.; Lu, S.-R.; Ding, W.-B.; Yu, X.-L.; Liang, G.-M.; Zou, J.-S.; Kang, F.-Y.; Zhang, J.-J.; Cao, Y.-D.  $\text{B}_2\text{O}_3/\text{LiBO}_2$  dual-modification layer stabilized Ni-rich cathode for lithium-ion battery. *J. Power Sources* **2022**, *536*, 231510. [[CrossRef](#)]
207. Hee, S.; Kang, S.; Lee, Y.-S.; Shin, W.-K.; Kim, S.; Shin, K.; Kim, D.-W. Improvement of the Cycling Performance of  $\text{LiNi}_{0.6}\text{Co}_{0.2}\text{Mn}_{0.2}\text{O}_2$  Cathode Active Materials by a Dual-Conductive Polymer Coating. *ACS Appl. Mater.* **2014**, *6*, 2546–2552.

208. Wu, Y.-S.; Pham, Q.-T.; Yang, C.-C.; Chern, C.-S.; Babulal, L.-M.; Seenivasan, M.; Jeyakumar, J.; Mengesha, T.-H.; Placke, T.; Brunklaus, G.; et al. Coating of a novel lithium-containing hybrid oligomer additive on nickel-rich  $\text{LiNi}_{0.8}\text{Co}_{0.1}\text{Mn}_{0.1}\text{O}_2$  cathode materials for high-stability and high-safety lithium-ion batteries. *ACS Sustain. Chem. Eng.* **2022**, *10*, 7394–7408. [[CrossRef](#)]
209. Xu, X.; Huo, H.; Jian, J.-Y.; Wang, L.-G.; Zhu, H.; Xu, S.; He, X.-S.; Yin, G.-P.; Du, C.-Y.; Sun, X.-L. Radially oriented single-crystal primary nanosheets enable ultrahigh rate and cycling properties of  $\text{LiNi}_{0.8}\text{Co}_{0.1}\text{Mn}_{0.1}\text{O}_2$  cathode material for lithium-ion batteries. *Adv. Energy Mater.* **2019**, *9*, 1803963. [[CrossRef](#)]
210. Wang, T.; Ren, K.-L.; He, M.; Dong, W.-H.; Xiao, W.; Pan, H.-Y.; Yang, J.; Yang, Y.; Liu, P.; Cao, Z.-J.; et al. Synthesis and Manipulation of Single-Crystalline Lithium Nickel Manganese Cobalt Oxide Cathodes: A Review of Growth Mechanism. *Front. Chem.* **2020**, *8*, 747. [[CrossRef](#)]
211. Liu, Y.-L.; Jessie, H.; Jeff, D. Microstructural Observations of “Single Crystal” Positive Electrode Materials Before and After Long Term Cycling by Cross-section Scanning Electron Microscopy. *J. Electrochem. Soc.* **2020**, *167*, 020512. [[CrossRef](#)]
212. Kong, X.-B.; Zhang, Y.-G.; Peng, S.-Y.; Zeng, J.; Zhao, J.-B. Superiority of single crystal to polycrystalline  $\text{LiNi}_x\text{Co}_y\text{Mn}_{1-x-y}\text{O}_2$  cathode materials in storage behaviors for lithium-ion batteries. *ACS Sustain. Chem. Eng.* **2020**, *8*, 14938–14948. [[CrossRef](#)]
213. Qian, G.-N.; Zhang, Y.-T.; Li, L.-S.; Zhang, R.-X.; Xu, J.-M.; Chen, Z.-J.; Xie, S.-J.; Wang, H.; Rao, Q.-L.; He, Y.-S.; et al. Single-crystal nickel-rich layered-oxide battery cathode materials: Synthesis, electrochemistry, and intra-granular fracture. *Energy Storage Mater.* **2020**, *27*, 140–149. [[CrossRef](#)]
214. Fan, X.-M.; Hu, G.-R.; Zhang, B.; Ou, X.; Zhang, J.-F.; Zhao, W.-G.; Jia, H.-P.; Zou, L.-F.; Li, P.; Yang, Y. Crack-free single crystalline Ni-rich layered NCM cathode enable superior cycling performance of lithium-ion batteries. *Nano. Energy* **2020**, *70*, 104450. [[CrossRef](#)]
215. Han, Y.-K.; Xu, J.-M.; Wang, W.; Long, F.; Qu, Q.; Wang, Y.; Zheng, H. Implanting an electrolyte additive on a single crystal Ni-rich cathode surface for improved cycle ability and safety. *J. Mater. Chem. A* **2020**, *8*, 24579–24589. [[CrossRef](#)]
216. Chen, X.; Tang, Y.; Fan, C.-L.; Han, S.-H. A highly stabilized single crystalline nickel-rich  $\text{LiNi}_{0.8}\text{Co}_{0.1}\text{Mn}_{0.1}\text{O}_2$  cathode through a novel surface spinel-phase modification. *Electrochim. Acta* **2020**, *341*, 136075. [[CrossRef](#)]
217. Zheng, L.-T.; Bennett, J.-C.; Obrovac, M.-N. All-dry synthesis of single crystal NMC cathode materials for Li-ion batteries. *J. Electrochem. Soc.* **2020**, *167*, 130536. [[CrossRef](#)]
218. Wang, F.; Ge, M.-Y.; Wi, S.-G.; Liu, X.; Bai, J.-M.; Steven, E.; Lu, D.-Y.; Lee, W.-K.; Chen, Z.-H.; Wang, F. Kinetic limitations in single-crystal high-nickel cathodes. *Angew. Chem. Int. Ed.* **2021**, *60*, 17350–17355.
219. Hu, J.-T.; Li, L.-Z.; Bi, Y.-J.; Tao, J.-H.; Lochala, J.; Liu, D.-Y.; Wu, B.-B.; Cao, X.; Chae, S.; Wang, C.-M.; et al. Locking Oxygen in Lattice: A Quantifiable Comparison of Gas Generation in Polycrystalline and Single Crystal Ni-Rich Cathodes. *Energy Storage Mater.* **2022**, *47*, 195–202. [[CrossRef](#)]
220. Zhao, W.-G.; Zou, L.-F.; Zhang, L.-T.; Fan, X.-M.; Zhang, H.-H.; Pagani, F.; Brack, E.; Seidl, L.; Ou, X.; Egorov, K.; et al. Assessing long-term cycling stability of single-crystal versus polycrystalline nickel-rich NCM in pouch cells with  $6 \text{ mAh} \cdot \text{cm}^{-2}$  Electrodes. *Small* **2022**, *18*, 2107357. [[CrossRef](#)]
221. Han, G.-M.; Kim, Y.-S.; Ryu, H.-H.; Sun, Y.-K.; Yoon, C.-H. Structural stability of single-crystalline Ni-rich layered cathode upon delithiation. *ACS Energy Lett.* **2022**, *7*, 2919–2926. [[CrossRef](#)]
222. Dai, P.-P.; Kong, X.-B.; Yang, H.-Y.; Li, J.-Y.; Zeng, J.; Zhao, J.-B. Single-crystal Ni-rich layered  $\text{LiNi}_{0.9}\text{Mn}_{0.1}\text{O}_2$  enables superior performance of co-free cathodes for lithium-ion Batteries. *ACS Sustain. Chem. Eng.* **2022**, *10*, 4381–4390. [[CrossRef](#)]
223. Kim, S.-Y.; Cha, H.; Kostecki, R.; Chen, G.-Y. Composite cathode design for high-energy all-solid-state lithium batteries with long cycle life. *ACS Energy Lett.* **2023**, *8*, 521–528. [[CrossRef](#)]
224. Huang, H.; Zhang, L.-P.; Tian, H.-Y.; Yan, J.-Q.; Tong, J.-F.; Liu, X.-H.; Zhang, H.-X.; Huang, H.-Q.; Hao, S.-M.; Gao, J.; et al. Pulse high temperature sintering to prepare single-crystal high nickel oxide cathodes with enhanced electrochemical performance. *Adv. Energy Mater.* **2023**, *13*, 2203188. [[CrossRef](#)]
225. Sun, Y.-K.; Myung, S.-T.; Kim, M.-H.; Prakash, J.; Amine, K. Synthesis and characterization of  $\text{Li}[(\text{Ni}_{0.8}\text{Co}_{0.1}\text{Mn}_{0.1})_{0.8}(\text{Ni}_{0.5}\text{Mn}_{0.5})_{0.2}]\text{O}_2$  with the microscale core-shell structure as the positive electrode material for lithium batteries. *J. Am. Chem. Soc.* **2005**, *127*, 13411–13418. [[CrossRef](#)]
226. Kim, M.-H.; Shin, H.-S.; Shin, D.; Sun, Y.-K. Synthesis and electrochemical properties of  $\text{Li}[\text{Ni}_{0.8}\text{Co}_{0.1}\text{Mn}_{0.1}]\text{O}_2$  and  $\text{Li}[\text{Ni}_{0.8}\text{Co}_{0.2}]\text{O}_2$  via co-precipitation. *J. Power Sources* **2006**, *159*, 1328–1333. [[CrossRef](#)]
227. Sun, Y.-K.; Myung, S.-T.; Park, B.-C.; Amine, K. Synthesis of spherical nano-to microscale core-shell particles  $\text{Li}[(\text{Ni}_{0.8}\text{Co}_{0.1}\text{Mn}_{0.1})_{1-x}(\text{Ni}_{0.5}\text{Mn}_{0.5})_x]\text{O}_2$  and their applications to lithium batteries. *Chem. Mater.* **2006**, *18*, 5159–5163. [[CrossRef](#)]
228. Sun, Y.-K.; Lee, B.-R.; Noh, H.-J.; Wu, H.; Myung, S.-T.; Amine, K. A novel concentration-gradient  $\text{Li}[\text{Ni}_{0.83}\text{Co}_{0.07}\text{Mn}_{0.10}]\text{O}_2$  cathode material for high-energy lithium-ion batteries. *J. Mater. Chem.* **2011**, *21*, 10108–10112. [[CrossRef](#)]
229. Myung, S.-T.; Noh, H.-J.; Yoon, S.-J.; Lee, E.-J.; Sun, Y.-K. Progress in High-Capacity Core-Shell Cathode Materials for Rechargeable Lithium Batteries. *J. Phys. Chem. Lett.* **2014**, *5*, 671–679. [[CrossRef](#)]
230. Li, Q.; Dang, R.; Chen, M.; Lee, Y.; Hu, Z.-B.; Xiao, X.-L. A synthesis method for long cycle life lithium-ion cathode material: Ni-rich core-shell  $\text{LiNi}_{0.8}\text{Co}_{0.1}\text{Mn}_{0.1}\text{O}_2$ . *ACS Appl. Mater. Interfaces* **2018**, *10*, 17850–17860. [[CrossRef](#)]
231. Chen, X.-L.; Jia, X.-B.; Qu, Y.-Y.; Li, D.; Chen, D.-M.; Chen, Y. High-voltage performance of concentration-gradient  $\text{Li}[\text{Ni}_{0.6}\text{Co}_{0.2}\text{Mn}_{0.2}]\text{O}_2$  layered oxide cathode materials for lithium batteries. *New J. Chem.* **2018**, *42*, 5868. [[CrossRef](#)]
232. Ryu, H.-H.; Park, N.-Y.; Noh, T.-C.; Kang, G.-C.; Maglia, F.; Kim, S.-J.; Yoon, C.-S.; Sun, Y.-K. Microstrain alleviation in high-energy Ni-rich NCM cathode for long battery life. *ACS Energy Lett.* **2021**, *6*, 216–223. [[CrossRef](#)]

233. Zheng, J.-C.; Yang, Z.; Dai, A.; Tang, L.-B.; Wei, H.-X.; Li, Y.-J.; He, Z.-J.; Lu, J. Boosting Cell Performance of  $\text{LiNi}_{0.8}\text{Co}_{0.15}\text{Al}_{0.05}\text{O}_2$  via Surface Structure Design. *Small* **2019**, *15*, 1904854. [[CrossRef](#)] [[PubMed](#)]
234. Bi, Y.-J.; Liu, M.; Xiao, B.-W.; Jiang, Y.; Lin, H.; Zhang, Z.-G.; Chen, G.-X.; Sun, Q.; He, H.-Y.; Huang, F.; et al. Highly stable Ni-rich layered oxide cathode enabled by a thick protective layer with bio-tissue structure. *Energy Storage Mater.* **2020**, *24*, 291–296. [[CrossRef](#)]
235. Park, G.-T.; Sun, H.-H.; Noh, T.-C.; Maglia, F.; Kim, S.-J.; Lamp, P.; Sun, Y.-K. Nanostructured co-free layered oxide cathode that affords fast-charging lithium-ion batteries for electric vehicles. *Adv. Energy Mater.* **2022**, *12*, 2202719. [[CrossRef](#)]
236. Rathore, D.; Garayt, M.; Liu, Y.-L.; Geng, C.-X.; Johnson, M.; Dahn, J.-R.; Yang, C.-Y. Preventing interdiffusion during synthesis of Ni-rich core-shell cathode materials. *ACS Energy Lett.* **2022**, *7*, 2189–2195. [[CrossRef](#)]
237. Sun, Y.-K.; Myung, S.-T.; Park, B.-C.; Prakash, J.; Belharouak, L.; Amine, K. High-energy cathode material for long-life and safe lithium batteries. *Nat. Mater.* **2009**, *8*, 320–324. [[CrossRef](#)]
238. Noh, H.-J.; Chen, Z.-H.; Yoon, C.-S.; Lu, J.; Amine, K.; Sun, Y.-K. Cathode Material with Nanorod Structure—An Application for Advanced High-Energy and Safe Lithium Batteries. *Chem. Mater.* **2013**, *25*, 2109–2115. [[CrossRef](#)]
239. Yoon, C.-S.; Sun, Y.K.; Kim, U.-H.; Park, K.-J.; Ryu, H.-H.; Kim, H.-S.; Sun, Y.-K. Microstructure Evolution of Concentration Gradient  $\text{Li}[\text{Ni}_{0.75}\text{Co}_{0.10}\text{Mn}_{0.15}]\text{O}_2$  Cathode for Lithium-Ion Batteries. *Adv. Funct. Mater.* **2018**, *28*, 1802090. [[CrossRef](#)]
240. Wu, K.; Wang, J.-Y.; Li, Q.; Yang, Y.-Q.; Deng, X.; Dang, R.-B.; Wu, M.-M.; Wu, Z.-J.; Xiao, X.-L.; Yu, X.-Q. In situ synthesis of nickel concentration gradient structure promising superior electrochemical properties of Ni-rich  $\text{LiNi}_{0.8}\text{Co}_{0.15}\text{Al}_{0.05}\text{O}_2$  at high cut-off voltage. *Nanoscale* **2020**, *12*, 11182–11191. [[CrossRef](#)]
241. Park, N.-Y.; Ryu, H.-H.; Park, G.-T.; Noh, T.-C.; Sun, Y.-K. Optimized Ni-rich NCMA cathode for electric vehicle batteries. *Adv. Energy Mater.* **2021**, *11*, 2003767. [[CrossRef](#)]
242. Shang, M.-W.; Chen, X.; Niu, J.-J. Nickel-rich layered  $\text{LiNi}_{0.8}\text{Mn}_{0.1}\text{Co}_{0.1}\text{O}_2$  with dual gradients on both primary and secondary particles in lithium-ion batteries. *Cell Rep. Phys. Sci.* **2022**, *3*, 100767. [[CrossRef](#)]

**Disclaimer/Publisher's Note:** The statements, opinions and data contained in all publications are solely those of the individual author(s) and contributor(s) and not of MDPI and/or the editor(s). MDPI and/or the editor(s) disclaim responsibility for any injury to people or property resulting from any ideas, methods, instructions or products referred to in the content.